



Object-oriented modeling, simulation and control of a 6-DoF parallel kinematic manipulator for remote handling in DONES facility

Claudio Tripodo^a, Stefano Lorenzi^a, Antonio Cammi^{a,*}, Gioacchino Micciché^b

^a Department of Energy, Nuclear Engineering Division, Politecnico di Milano, Via La Masa 34, Milan 20156, Italy

^b ENEA, ENEA CR Brasimone, Località Brasimone, Camugnano (BO) 40032, Italy

ARTICLE INFO

Keywords:

Modeling
Simulation
Control
Robot
Modelica
Dymola
Object-oriented
Dynamics
Parallel manipulator
Stewart platform
DONES
Remote handling
PID

ABSTRACT

This paper describes the modeling and simulation activities performed, within the EUROfusion framework, to support the engineering design and the development of the control system of the DONES Parallel Kinematic Manipulator (PKM), a 6-DoF parallel robot part of the Remote Handling System of the DONES facility. The main tasks of the PKM are the planned annual replacement of the Target Assembly and the High Flux Test Module, two of the crucial and most activated components of DONES. The PKM model, developed using the Modelica object-oriented language, is able to simulate the dynamics of the entire robots, including the main non-linear effects due to backlashes and static friction. The simulator is employed to support the preliminary design of the control system, based on an independent-joint approach with dual-loop cascade-PID logic. Simulations are then conducted to assess robot performances in terms of resolution, accuracy, repeatability and generated forces.

Acronyms

DEMO	DEMONstration Power Plant
DoF	Degree of Freedom
DONES	Demo-Oriented NEutron Source
EMA	Electro-Mechanical Actuator
ESFRI	European Strategy Forum on Research Infrastructures
EU	European Union
HFTM	High Flux Test Module
IFMIF	International Fusion Material Irradiation Facility
ITER	International Thermonuclear Experimental Reactor
LTI	Linear Time-Invariant
PID	Proportional-Integral-Derivative
PKM	Parallel Kinematic Manipulator
PMSM	Permanent Magnet Servo Motor
RH	Remote Handling
RHS	Remote Handling System
RMS	Root Mean Squared
SISO	Single-Input Single-Output
TA	Target Assembly

TC Test Cell

Latin symbols

b_{li}	legs vectors
c_i	cosine of i th angle component
C_{ti}	mobile platform spherical joints position vectors
F	mobile platform force
g	gravity vector
GC	center of mass vector
\bar{I}	inertia tensor
I_q	motor current, quadrature component
\bar{I}_3	identity matrix, 3-th order
\bar{J}_k	kinematic Jacobian matrix
J_m	motor inertia
K_T	torque constant
L_D	effective inductivity
m	mass
M	obile Platform moment
M_M	motor torque

* Corresponding author.

E-mail address: antonio.cammi@polimi.it (A. Cammi).

Ob_i	Fixed Base Universal joints position vectors
OC	mobile platform position vector
p	number of motor pole pairs
q	legs lengths vector
R	winding resistance
\bar{R}	mobile platform rotation matrix
S	mobile platform task-space pose vector
s_i	sine of i th angle component
u_a	generic motor variable, a-axis component
u_b	generic motor variable, b-axis component
u_c	generic motor variable, c-axis component
u_d	generic motor variable, direct component
u_q	generic motor variable, quadrature component
u_0	generic motor variable, 0-axis component
U_d	motor voltage, direct component
U_q	motor voltage, quadrature component
V	mobile platform translation velocity
W	mobile platform wrench
x_C	mobile platform pose, x-coordinate
y_C	mobile platform pose, y-coordinate
z_C	mobile platform pose, z-coordinate

Greek symbols

θ	mobile platform pose, x-angle
θ_r	motor rotor angle
τ	actuators forces vector
τ_{centr}	actuators forces vector, centrifugal/Coriolis component
τ_{grav}	actuators forces vector, gravitational component
τ_i	force on i -th actuator
τ_{iner}	actuators forces vector, inertial component
φ	mobile platform pose, y-angle
ϕ	mobile platform pose, z-angle
ψ_{PM}	permanent-magnet magnetic flux
ω_M	motor rotor speed
Ω	mobile platform rotation velocity

1. Introduction

The IFMIF-DONES (International Fusion Materials Irradiation Facility - DEMO-Oriented NEutron Source [1,2], from here on only “DONES”) project is – together with ITER (International Thermonuclear Experimental Reactor) and DEMO (DEMONstration Power Plant) – one of the three main projects in the EU R&D programme towards the commercial use of nuclear fusion energy. Due to its strategic potential and impact on European research, DONES has been included in the ESFRI Roadmap 2018 (European Strategy Forum on Research Infrastructures [3],) as one of the activities that European scientific community has identified as being of the highest level for carrying out strategic scientific research activities and achieving excellence in technological innovation.

The irradiation environment in future Fusion Power Plants (and obviously also in DEMO independently of its specific design) is characterized by the presence of 14 MeV fusion neutrons in the first wall area: understanding the degradation of the materials and components properties throughout the reactor operational life is a key issue to allow the design and subsequent facility licensing by the corresponding safety authorities. The mission of DONES [1] is to provide a neutron source producing high energy neutrons at sufficient intensity and irradiation volume in order to generate materials irradiation test data for design, licensing, construction and safe operation of DEMO, as well as to generate a data base for benchmarking of radiation responses of materials.

DONES Plant will achieve its goal by means of an accelerator-based D-Li neutron source to simulate as closely as possible the first wall neutron spectrum of future nuclear fusion reactors. The conceptual scheme of DONES is shown in Fig. 1. DONES accelerator will produce a 125 mA deuteron beam that, accelerated up to 40 MeV and shaped to have a proper nominal cross section, impinges on a liquid lithium curtain 25 mm thick cross-flowing at about 15 m/s in front of it in the Target System. The stripping reactions generate a large number of neutrons that interact with the materials samples located immediately

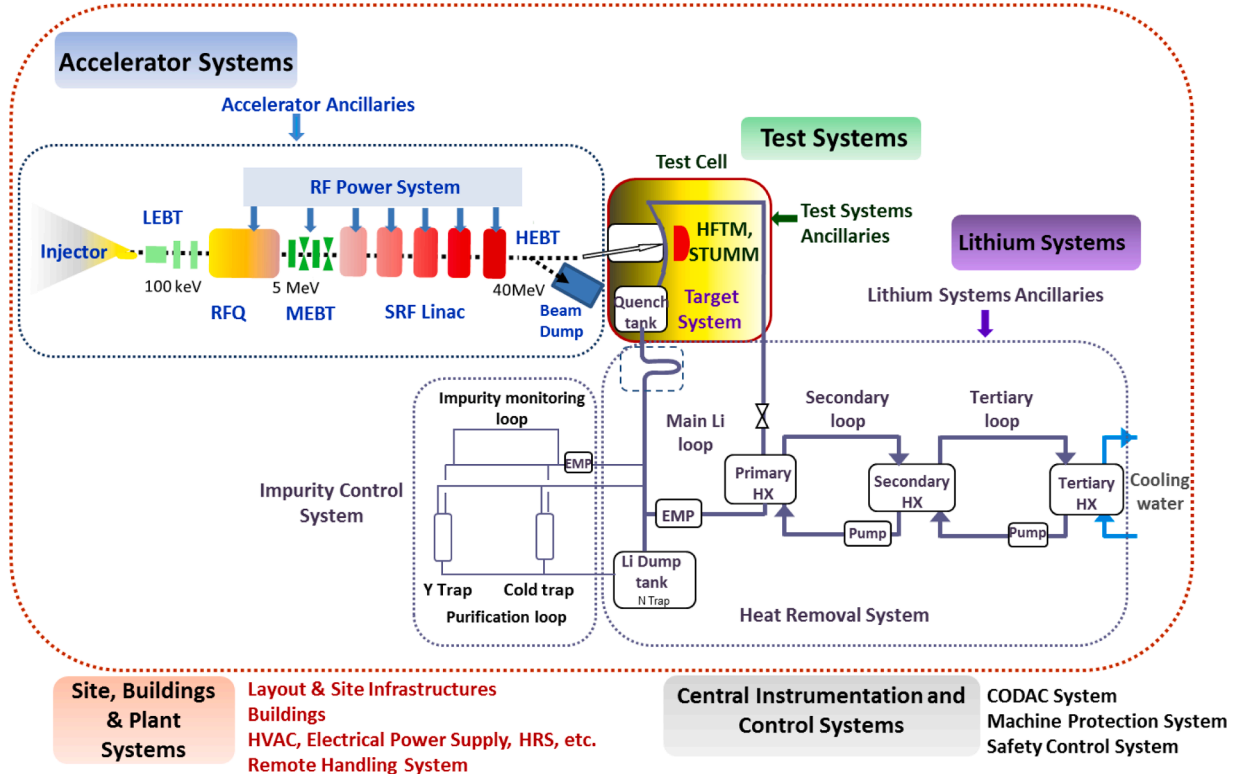


Fig. 1. DONES schematic Plant configuration [1].

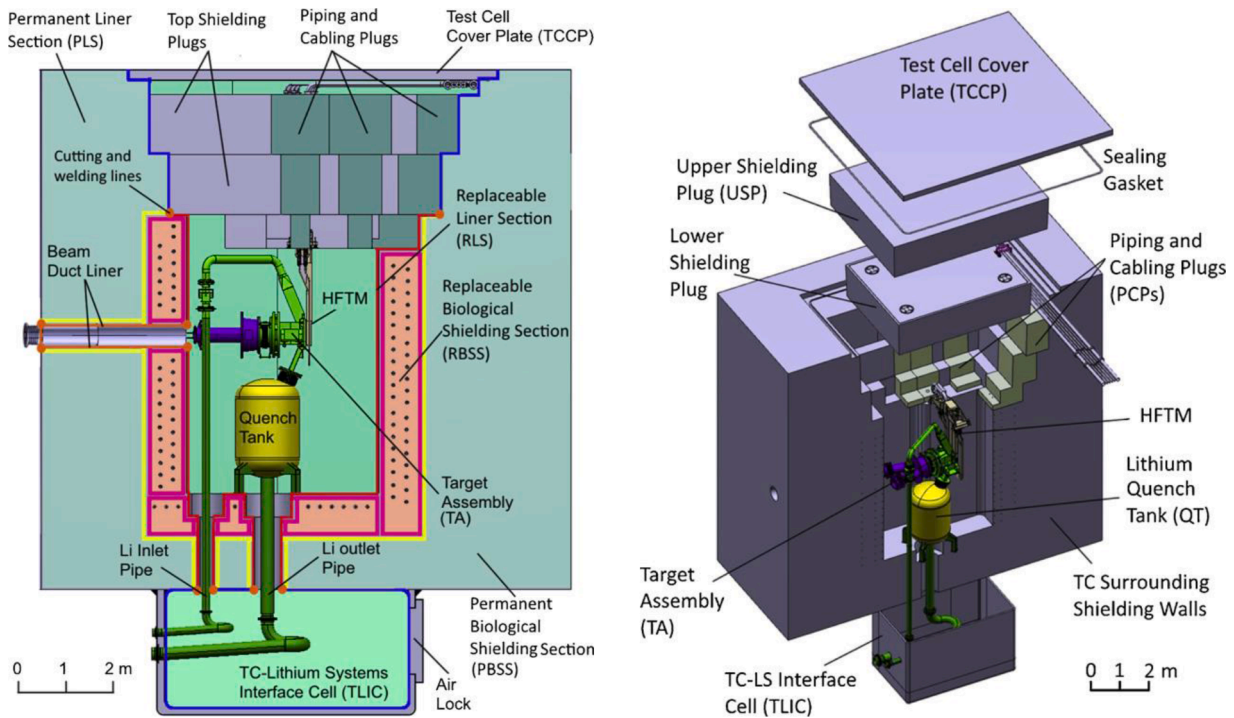


Fig. 2. Side (left) and isometric (right) views of the Test Cell of DONES [4].

behind the Lithium Target, in the High-Flux Test Module (HFTM). A view of the Test Cell (TC), where Target System and HFTM are located, can be seen in Fig. 2.

Due to the severe radiation levels caused by neutron activation, maintenance and inspection activities in several areas of the DONES Plant has to be carried out in a fully remotized way. The main tasks of the Parallel Kinematic Manipulator (PKM) robot – which is part of the Remote Handling System (RHS) of DONES – are the planned annual replacement of the Target Assembly (TA) and the High Flux Test Module (HFTM), two of the most activated components of the DONES facility. These operations present very stringent requirements in terms of positioning and inclination resolution and payload, as well as strong constraints in terms of weight and dimensions of the robot due to the tightly packed environment of the Test Cell of DONES (Fig. 2).

These requirements have led to the adoption of a parallel robot architecture [5], which presents several favorable features with respect to the conventional serial “anthropomorphic” design. In particular, the 6-DoF Stewart (or Gough-Stewart) platform [6] kinematic architecture has been selected in order to allow the full control of the payload position (x , y , z) and inclination (roll, pitch, yaw). The DONES PKM is an “upside-down” version of the classic Stewart platform. The upper base is held fixed during operation, while the lower platform, which constitutes the robot’s end-effector, is translated and rotated by means of the actuation of the six adjustable-length legs. Stewart-platform-based robots have encountered, in the last couple of decades, a large interest in both research and industry. They have been employed in the fields of robotics, flight simulation, underwater research, satellite antennas positioning and orthopedic surgery [5]. Most of recent research work has been devoted to forward kinematics [7,8], dynamics [9], workspace and singularities analysis [10], and control [11]. In this work, the focus is put on analyzing the impacts that nonlinearities (backlashes and static friction) and elasticity have on robot resolution, accuracy and repeatability, and on developing and assessing the effectiveness of motion control strategies.

Modeling & simulation activities are essential tasks in the design process of robots and manipulators. Scope of this paper is the description of the modeling and simulation activities performed, within the

framework of the EUROfusion Consortium, to support the preliminary engineering design of the PKM and the preliminary development of its control system. The model developed is able to reproduce the dynamics of the actuators (electric motors, inertias, elasticities) including the non-linear effects due to backlashes and static friction (in gearings, transmissions and ballscrews). The latter two are crucial aspects for the impact they have on robot resolution and on the definition of control algorithms. In this paper, an object-oriented approach has been employed in the modeling of the PKM device by means of the Modelica language [12]. Modelica is an object-oriented, declarative, equation-based language developed for the component-oriented modeling of complex physical and engineering systems. It allows a description of single components directly in terms of physical equations and principles. Different components can then be connected through standardized interfaces (or “connectors”). Modelica is open-source and it offers an ample, built-in standard library [13], which include components of mechanical, electromagnetic, and thermo-fluid domains. In addition, a large number of validated proprietary libraries are available (e.g. ElectricPowerSystem and WindPower from Dassault Systemes [14]). Modelica has already been successfully adopted for modeling systems within different fields, such as automotive [15], robotics [16], thermo-hydraulics [17], electrical [18], and nuclear energy [19,20]. Modelica-based models have been employed as system-dynamics simulators to support control design [21,22]. In this paper, the Dymola [14] environment is used as simulation tool, although open-source alternatives are available, e.g. OpenModelica [23].

The paper is organized as follows: after this introduction, Section 2 presents a brief description of the PKM in the context of the Remote Handling System of DONES, Section 3 describes the modeling approach adopted in developing the PKM simulator, Section 4 describes the development of the PKM control system, Section 5 presents some simulation results, and in Section 6 a few conclusions are drawn.

2. The PKM in DONES Remote Handling System

The DONES Remote Handling (RH) System [24] is a man-in-the-loop system for performing remote maintenance tasks on the DONES [25]

Table 1
Main requirements of the PKM.

Parameter	Requirement
Degrees of Freedom	6 (X,Y,Z,RX,RY,RZ)
Design payload	1300 kg
Maximum proper weighth	1000 kg
Translation (X,Y,Z)	
Accuracy/repeatability	0.5 mm
Resolution	0.05 mm
Velocity	4 mm/s
Rotation (RX,RY,RZ)	
Accuracy/repeatability	0.1°
Resolution	0.01°
Velocity	0.2 °/s

machine and machine components. The Parallel Kinematic Manipulator (PKM) is a robotic device performing RH activities within the DONES Test Cell, the most activated area of the DONES facility. In particular, the PKM is responsible for positioning and removal of the Target Assembly (TA) and the High Flux Test Module (HFTM) in/from the Test Cell (TC,

see Fig. 2), a task requiring the manipulation of large loads with high position and inclination resolution in a tightly packed environment and with stringent weight and size requirements (main requirements are reported in Table 1). These operating conditions lead to the adoption of a parallel robot topology, in which the robot end-effector is directly connected to the base by several independent linkages working simultaneously. In comparison with the more conventional serial (or “anthropomorphic”) topology, parallel robots offer higher positioning accuracy, higher mechanical stiffness and higher payload-capacity/robot-mass ratio. The PKM (Fig. 3) is essentially an “upside-down” version of the classic Stewart (or Stewart-Gough) Platform, a 6-DoF robot allowing full end-effector positioning (x, y, z) and orientation (Rx, Ry, Rz) capability. The pose of the end-effector (which, for the PKM, is here called Mobile Platform) is adjusted by means of six parallel and identical variable-length legs, based on electromechanical linear actuators. The PKM can also be identified as a 6-UPS robot, where U (Universal), P (Prismatic) and S (Spherical) indicate the typology of the joints that constitute the kinematics of the legs. The notation employed in the following of this paper, together with the main

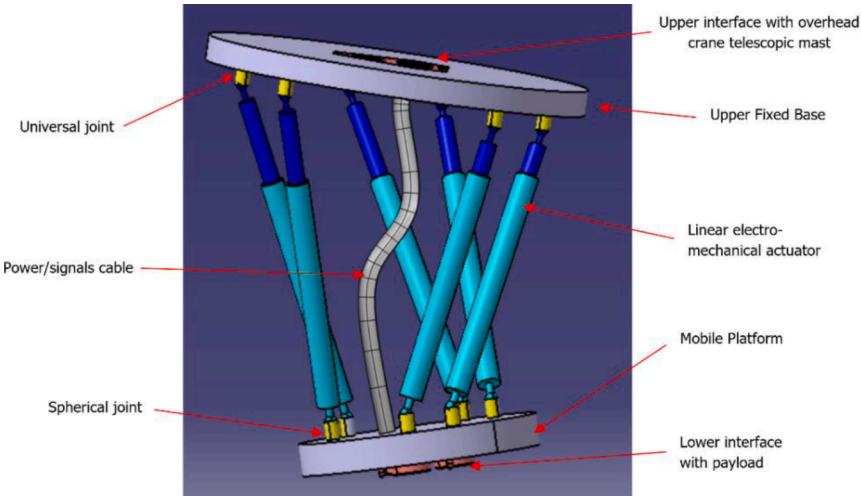


Fig. 3. Conceptual model of the PKM.

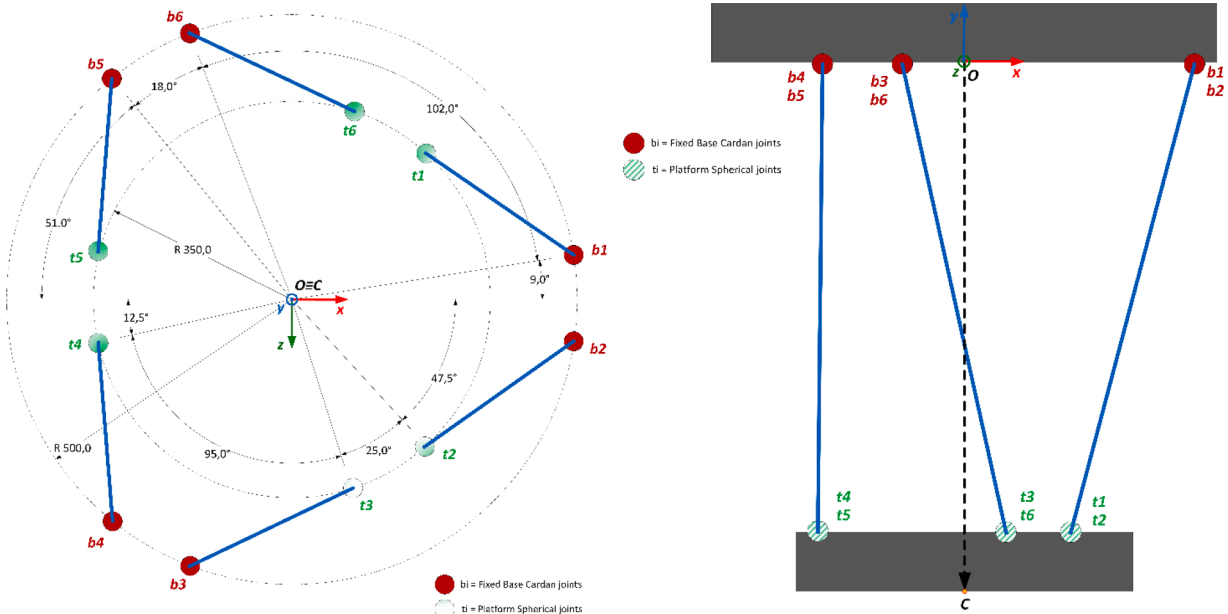


Fig. 4. PKM notation and dimensions, top (left) and side (right) views.

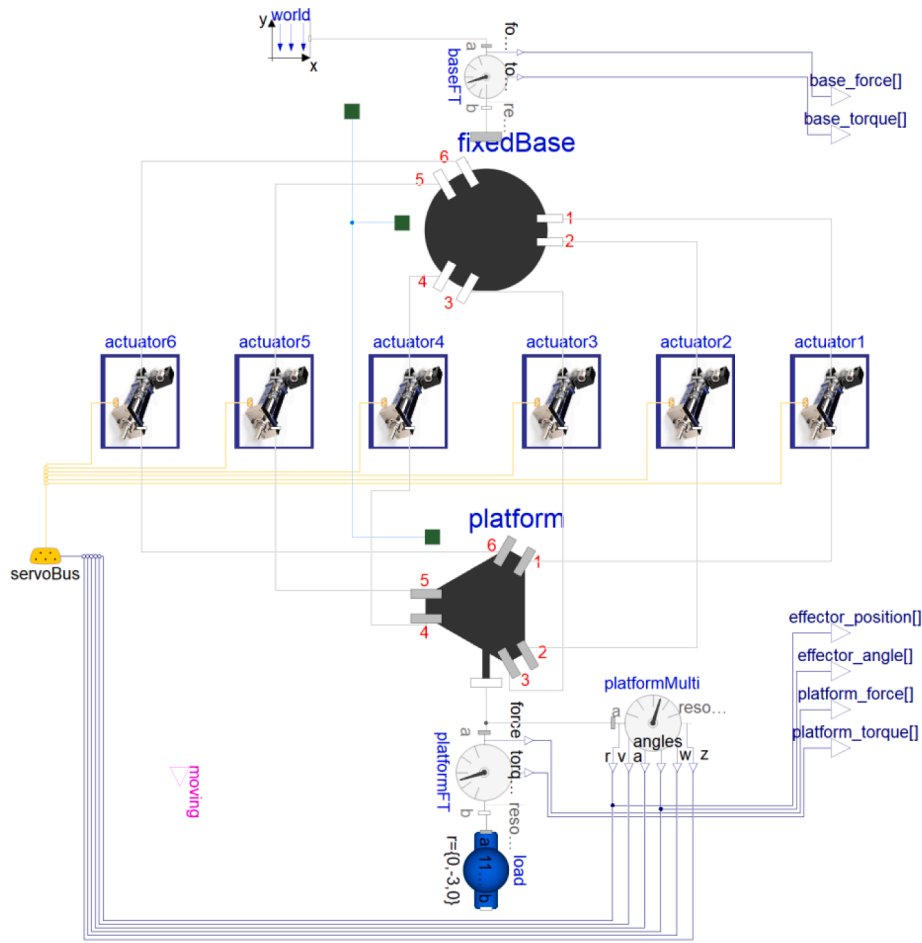


Fig. 5. Modelica model of the PKM device.

dimensions, are shown in Fig. 4.

The environmental conditions of the DONES Test Cell during PKM deployment are characterized by Argon atmosphere and a maximum temperature of 80 °C. The maximum dose rate in the Test Cell during PKM operation is of the order of 100 Gy/h, with an expected cumulative dose of several tens of kGy per replacement cycle (of TA and HFTM), and up to 1 MGy lifetime cumulative dose. During its operation, the PKM is deployed in the DONES Test Cell by means of a telescopic mast of one of the overhead cranes of the DONES facility. The large part of the motion is performed by the overhead crane (in x-z plane) and the telescopic mast (in the vertical y-direction), while the PKM is responsible of the final high-resolution positioning and inclination of the payload. The interfaces between the PKM and the telescopic mast, and between the PKM and the payloads, allow for remote automatic connection/disconnection of the devices. They also provide the required pass-throughs modules for signals and power cabling connections (as well as other utilities, e.g. pneumatic supply). The limited number of pass-throughs connections imposes the adoption of multiplexed communication between the control cabinet and the robot, with some implications on robot control (see Section 4).

3. PKM simulator description

This section describes the modeling approach employed for the Modelica PKM simulator. The simulator includes a non-linear multibody dynamic model of the PKM device, a trajectory generation module, a module deputed to perform kinematics and dynamics computations needed for robot control, the motion controller model, and an input/output module for signal multiplexing. The different components are

described in the following of this section. The simulator has been developed using the object-oriented Modelica language. The model makes use of the Modelica Standard Library [13] (in particular the Multibody, Rotational and Translational components of the Mechanics Library), the Modelica LinearSystems2 [26] (employed for discrete-time control modeling), and the FeedDriveLibrary [27] (for modeling of the electric motors).

3.1. PKM device

The Modelica multibody 3D model of the PKM device is shown in Fig. 5. In accordance with the object-oriented philosophy, it has been built by assembling the subcomponents of the Fixed Base (*fixedBase* in Fig. 5), the six actuated legs (*actuator1* through *actuator6*), the Mobile Platform (*platform*) and the payload (*load*), which are described in more detail in the following of this Section. The subcomponents are interfaced with each other via mechanical connectors, which contain the equations describing the fixed mechanical coupling (position, orientation, and transmitted forces and torques). In addition to the mechanical components, a number of ideal sensors are present: *baseFT* (which measures forces and moments on the Fixed Base), *platformFT* (which measures forces and moments on the Mobile Platform) and *platformMulti* (which measures linear and angular positions, velocities and accelerations of the Mobile Platform). A bus for signals multiplexing (*servoBus*) is also included in the PKM model.

3.1.1. Fixed base

The Fixed Base model (Fig. 6) is a simple geometrical model which establishes the spatial coordinates of the six universal joints (*frame_1*

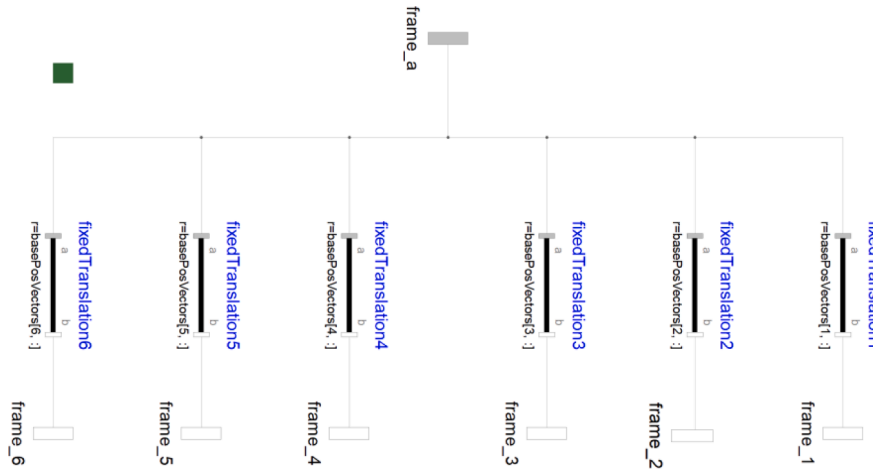


Fig. 6. Modelica model of the Fixed Base.

Table 2

Coordinates of the universal joints on the Fixed Base.

Universal joint #	x-coordinate (m)	y-coordinate (m)	z-coordinate (m)
1 ($\overline{Ob_1}$)	0.4938	0.0000	-0.0782
2 ($\overline{Ob_2}$)	0.4938	0.0000	0.0782
3 ($\overline{Ob_3}$)	-0.1792	0.0000	0.4668
4 ($\overline{Ob_4}$)	-0.3147	0.0000	0.3886
5 ($\overline{Ob_5}$)	-0.3147	0.0000	-0.3886
6 ($\overline{Ob_6}$)	-0.1792	0.0000	-0.4668

connected. As can be seen from Fig. 5, *frame_a* of the Fixed Base is connected to the *world* component, which provides the absolute reference coordinate system. An ideal sensor for 3-axis force and torque (*baseFT*) is also included¹. The coordinates of the Fixed Base universal joints (*basePosVectors*[*i*,:] in Fig. 6) are reported in Table 2.

3.1.2. Mobile platform

In analogy with the Fixed Base (Section 3.1.1), the Mobile Platform model (Fig. 7) establishes the spatial coordinates of the six spherical joints (Table 3). The *platformBody* component implements the equations

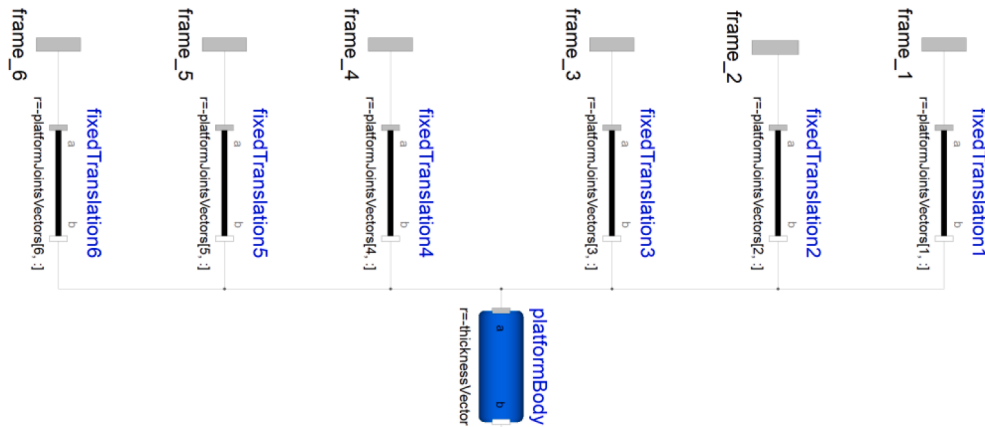


Fig. 7. Modelica model of the Mobile Platform.

Table 3

Coordinates of the spherical joints on the Mobile Platform in the reference starting pose.

Spherical joint #	x-coordinate [m]	y-coordinate [m]	z-coordinate [m]
1 ($\overline{Ct_1}$)	0.2365	0.1200	-0.2580
2 ($\overline{Ct_2}$)	0.2365	0.1200	0.2580
3 ($\overline{Ct_3}$)	0.1052	0.1200	0.3338
4 ($\overline{Ct_4}$)	-0.3417	0.1200	0.0758
5 ($\overline{Ct_5}$)	-0.3417	0.1200	-0.0758
6 ($\overline{Ct_6}$)	0.1052	0.1200	-0.3338

through *frame_6*) with respect to the origin of the PKM coordinate system (*frame_a*) by means of the *fixedTranslation* multibody component of the Modelica Standard Library. This component implements a fixed 3D rigid translation (with no rotation) between the two frames to which it is

describing a rigid body with fixed mass, center of mass and inertia tensor. The *BodyCylinder* multibody component of the Modelica Standard Library has been employed (i.e., the Mobile Platform is approximated as a cylinder). Geometrical and physical data are reported in Table 4. The Mobile Platform is equipped (Fig. 5) with ideal sensors for 3-axis force and torque (*platformFT*) and for translational and rotational position, velocity and acceleration (*platformMulti*)².

¹ Signals of forces and torques acting on the Fixed Base's interface with the telescopic mast are needed for robot contact detection and machine protection. These aspects are not treated in detail in this paper.

² Note that these sensors do not correspond to physical sensors installed on the robot. They are included in the PKM model for computational reasons (essentially, to provide robot Forward Kinematics resolution).

Table 4
Physical properties of the Mobile Platform.

Parameter	Value	unit
Mass	323.27	kg
C.o.G. coordinates	[0, 0.060, 0]	m
Inertia tensor xx	10.288	kg·m ²
Inertia tensor yy	19.800	kg·m ²
Inertia tensor zz	10.288	kg·m ²

Table 5
Physical properties of the Load component.

Parameter	Value	Unit
Mass	1154.54	kg
C.o.G. coordinates	[0, 1.500, 0]	m
Inertia tensor xx	901.26	kg·m ²
Inertia tensor yy	70.72	kg·m ²
Inertia tensor zz	901.26	kg·m ²

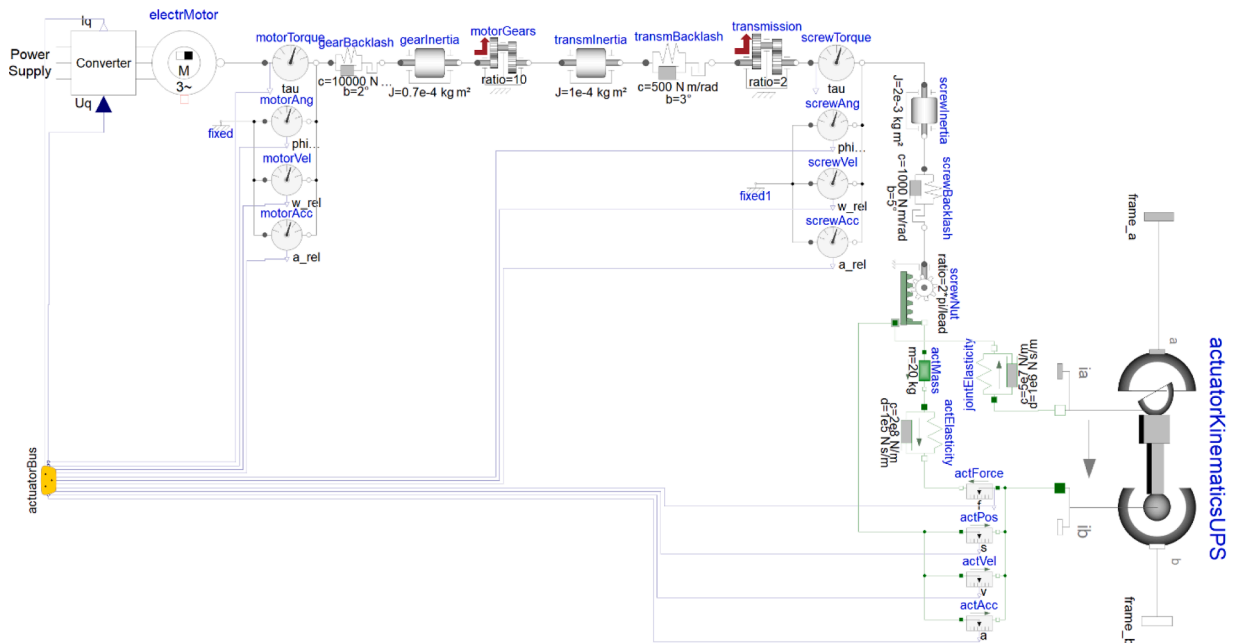


Fig. 8. Modelica model of the linear electromechanical actuator.

3.1.3. Load

The *load* component represents the payload of the PKM. It is modeled as a rigid body with fixed mass, center of mass and inertia tensor by employing the *BodyShape* multibody component of the Modelica Standard Library (which can be used to model a rigid body of generic shape). Geometrical and physical parameters, which refer to the TA data available at time of writing, are reported in Table 5.

3.1.4. Servo bus

The *servoBus* component is a Modelica connector³ employed for signal multiplexing, i.e. to transmit input/output signals from/to the individual actuators.

3.1.5. Actuators

The six *actuators* components represent the six actuated legs of the

PKM. Each leg is constituted by a linear Electro-Mechanical-Actuator (EMA) based on ballscrew or roller-screw technology for converting electric motors' rotation to linear motion. The actuator Modelica model is shown in Fig. 8. Model parameters are summarized in Table 6⁴. As will be described in this subsection, the actuator's model includes components reproducing the dynamics of electric motors, inertias, elasticities, and the non-linear effects due to backlashes and static friction (in gearings, transmissions, and screws). The latter two are crucial aspects for the impact they have on robot resolution and on the definition of control algorithms.

Legs kinematics. The *actuatorKinematicsUPS* component on the right of Fig. 8 (an instance of the *JointUPS* multibody component of the Modelica Standard Library) implements the equations of a kinematic chain consisting of a Universal joint (U, 2 rotational DoF) at *frame_a*, a Spherical joint (S, 3 rotational DoF) at *frame_b*, and a Prismatic joint (P, 1 translational DoF) along the line connecting the origins of the two frames. This joint aggregation has no mass and no inertia and introduces

neither constraints nor potential state variables. The prismatic joint is actuated (i.e., its lengths can be adjusted by action of the motors), while the upper Universal and the lower Spherical joints are passive.

Electric servomotor. The *electrMotor* component implements the equations of a Permanent Magnet Servo-Motor (PMSM), and it is based on the *PMSM* component of the Modelica FeedDriveLibrary [27]. It is a simplified motor model which adopts the direct-quadrature (dq) coordinate system for electromagnetic variables (Fig. 9). The equivalent simplified circuit is shown in Fig. 10.

The constitutive equations of the motor are reported in Eq. (1):

³ Connectors are a particular typology of Modelica components which can only be employed for communication of variables between components, and cannot contain equations.

⁴ It should be noticed that Modelica allows to easily modify model's parameters (Table 6, and previous Tables 5, 4, 3 and 2) at runtime. The present model can thus be easily updated and tuned against experimental and validation data.

Table 6
Parameters of the components of the linear EMA

Parameter	Value	Unit
Motor		
Rated torque	1.2	N·m
Rated speed	3000	rpm
Rated current	2.0	A
Torque constant	0.6	N·m·A ⁻¹
Winding resistance at 20°C	20	Ω
Effective inductivity	5·10 ⁻³	H
Number of pole pairs	1	-
Rotor inertia	0.5·10 ⁻⁴	kg·m ²
Gears		
Ratio	10	-
Static friction	0.1	N·m
Coulomb friction	0.05	N·m
Proportional friction	2·10 ⁻⁴	N·m·s·rad ⁻¹
Efficiency	90	%
Coupling backlash	2	°
Elasticity	10 ⁴	N·m·rad ⁻¹
Damping	0.1	N·m·s·rad ⁻¹
Inertia	0.7·10 ⁻⁴	kg·m ²
Transmission belt		
Ratio	2	-
Backlash	3	°
Elasticity	500	N·m·rad ⁻¹
Damping	1	N·m·s·rad ⁻¹
Inertia	10 ⁻⁴	kg·m ²
Ballscrew		
Screw lead	5	mm
Ratio	1256.64	rad·m ⁻¹
Static friction	1	N·m
Coulomb friction	0.5	N·m
Proportional friction	10 ⁻²	N·m·s·rad ⁻¹
Efficiency	80	%
Rotational backlash	5	°
Rotational elasticity	1000	N·m·rad ⁻¹
Rotational damping	0.5	N·m·s·rad ⁻¹
Rotational inertia	20·10 ⁻⁴	kg·m ²
Thrust tube elasticity	2·10 ⁸	N·m ⁻¹
Thrust tube damping	1·10 ⁵	N·s·m ⁻¹
Mass	20	kg

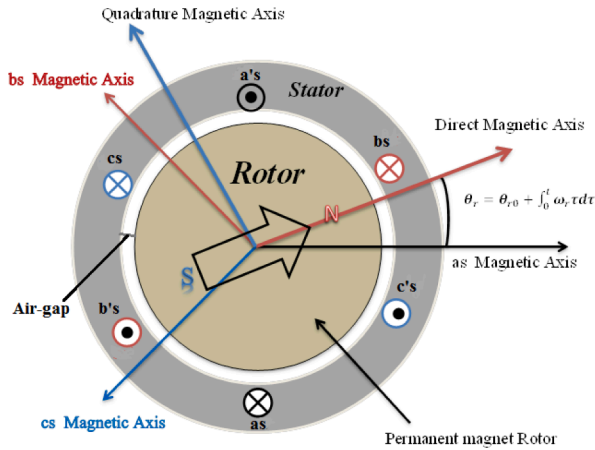


Fig. 9. Coordinates systems of the PMSM.

$$\begin{cases} U_d = -p \cdot \omega_M \cdot L_D \cdot I_q \\ U_q = L_D \frac{dI_q}{dt} + R \cdot I_q + p \cdot \omega_M \cdot \psi_{PM} \\ M_M = 3 \cdot p \cdot \psi_{PM} \cdot I_q \\ \psi_{PM} = \frac{1}{3 \cdot p} K_T \end{cases} \quad (1)$$

where U_d , U_q and I_q are the RMS values of the motor voltage and torque-building current in the dq-frame, and ω_M is the angular velocity of the rotor. The number of pole pairs p , the effective inductivity L_D and the winding resistance R can be taken from motor supplier data. The magnetic flux of the permanent-magnet ψ_{PM} relates, via the torque constant K_T , the motor torque M_M and the torque-building current I_q . In the constitutive equations it is assumed, as common practice, that the stator direct current I_d is kept at zero by the motor controller. The relationship between the variables expressed in the dq-frame (u_d , u_q , u_0) and the corresponding three-phase quantities (u_a , u_b , u_c , in the abc-frame) is expressed by the Park transformation Eq. (2) [28], where ϑ_r is the rotor angle. The PMSM Modelica model is shown in Fig. 11.

$$\begin{bmatrix} u_d \\ u_q \\ u_0 \end{bmatrix} = \frac{2}{3} \begin{bmatrix} \cos(\vartheta_r) & \cos\left(\vartheta_r - \frac{2\pi}{3}\right) & \cos\left(\vartheta_r + \frac{2\pi}{3}\right) \\ -\sin(\vartheta_r) & -\sin\left(\vartheta_r - \frac{2\pi}{3}\right) & -\sin\left(\vartheta_r + \frac{2\pi}{3}\right) \\ \frac{1}{2} & \frac{1}{2} & \frac{1}{2} \end{bmatrix} \begin{bmatrix} u_a \\ u_b \\ u_c \end{bmatrix} \quad (2)$$

The adoption of this motor model relies on the fact that it can be easily parametrized with readily available motor-supplier data. On the other hand, at the detail level of the present model, it can be considered that the un-modeled dynamics (e.g. torque ripple) do not affect the resolution and accuracy of the overall PKM model thanks to the high transmission ratio of the EMA. For computational reasons, friction in the motor model is set to zero; the resulting total friction of the motor-gear assembly is dealt with in the *motorGears* component (see Section 3.1.5.3). Values employed for motor parameters are reported in Table 6.

Gearing and transmission. The *motorGears* and *transmission* components model the motor integrated gearing and the transmission of the EMA in parallel-motor configuration, respectively. These components are instances of the *LossyGear* mechanical component of the Modelica Standard Library, which models the gear ratio, the friction and the losses of a standard gear box in a realistic way. Friction in particular is modeled in a physically meaningful way, taking into account that at zero speeds the movement may be locked due to static friction in the gear teeth and/or in the bearings. Friction characteristics can be specified in a velocity-dependent tabular format, thus allowing accurate implementation of the Stribeck friction curve (Fig. 12). Table 6 shows the parameters employed for the *motorGears* and *transmission*⁵ components.

Inertia. The *Inertia* mechanical component of the Modelica Standard Library is employed to model the rotational inertia of the transmission (*transmInertia*) and the screw shaft (*screwInertia*), together with the associated bearings.

Backlash and elasticity. The *gearBacklash*, *transmBacklash* and *screwBacklash* components are used to model the backlashes and the elasticity of the motor-gear coupling, the transmission belt and the screw assembly. They are based on the *ElastoBacklash* mechanical rotational

⁵ Note that, for computational reasons, the *transmission* element also includes the friction contribution from the screw nut assembly. This allows to model the latter as an ideal (friction-less) element, see Section 3.1.5.6.

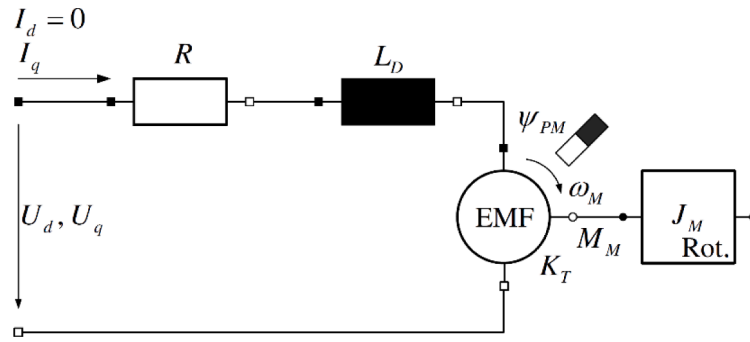


Fig. 10. Simplified circuit of the PMSM.

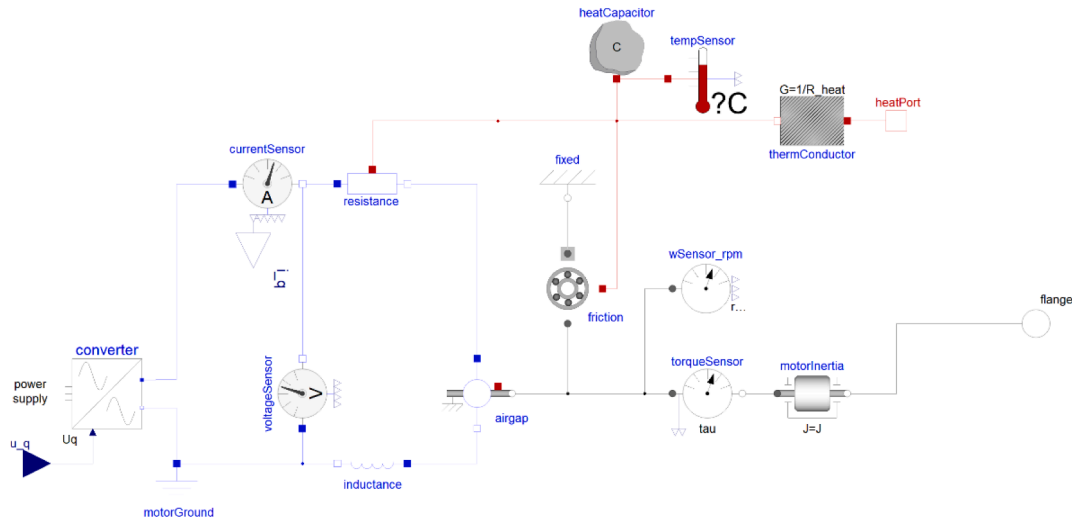


Fig. 11. Modelica model of the PMSM of the FeedDriveLibrary [27].

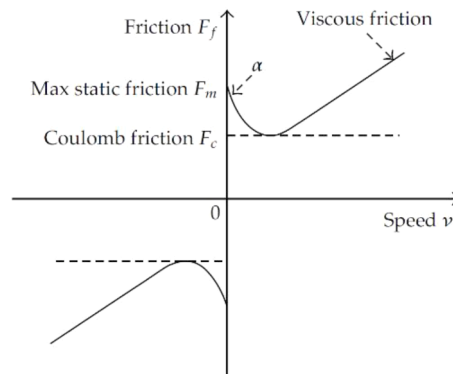


Fig. 12. Stribeck friction characteristics.

component of the Modelica Standard Library. This element consists of a backlash element connected in series to a parallel spring-and-damper element. In the backlash region no torque is exerted. Outside of this region, contact is present and the contact torque is basically computed with a linear spring/damper characteristic. The *actElasticity* and *jointElasticity* components model the translational elasticity of the actuator's

thrust tube and of the legs' Universal and Spherical joints assemblies, respectively. They consist of *SpringDamper* mechanical components of the Modelica Standard Library, which implements the equation of a parallel-spring-and-damper system. Table 6 shows the parameters employed for the four components.

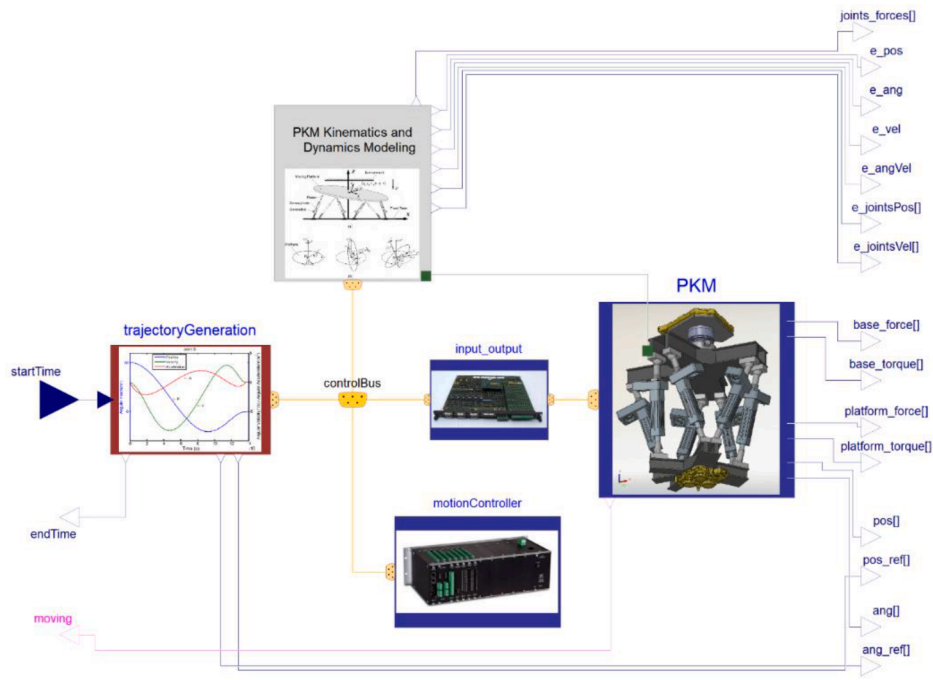


Fig. 13. Modelica model of the PKM simulator.

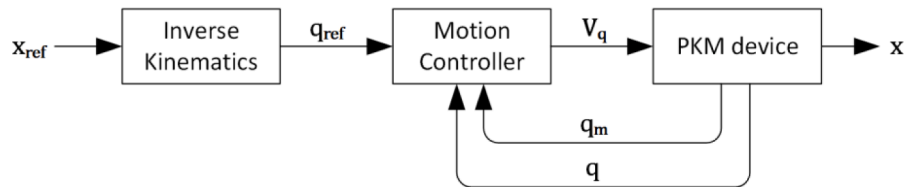


Fig. 14. Joint-space control scheme.

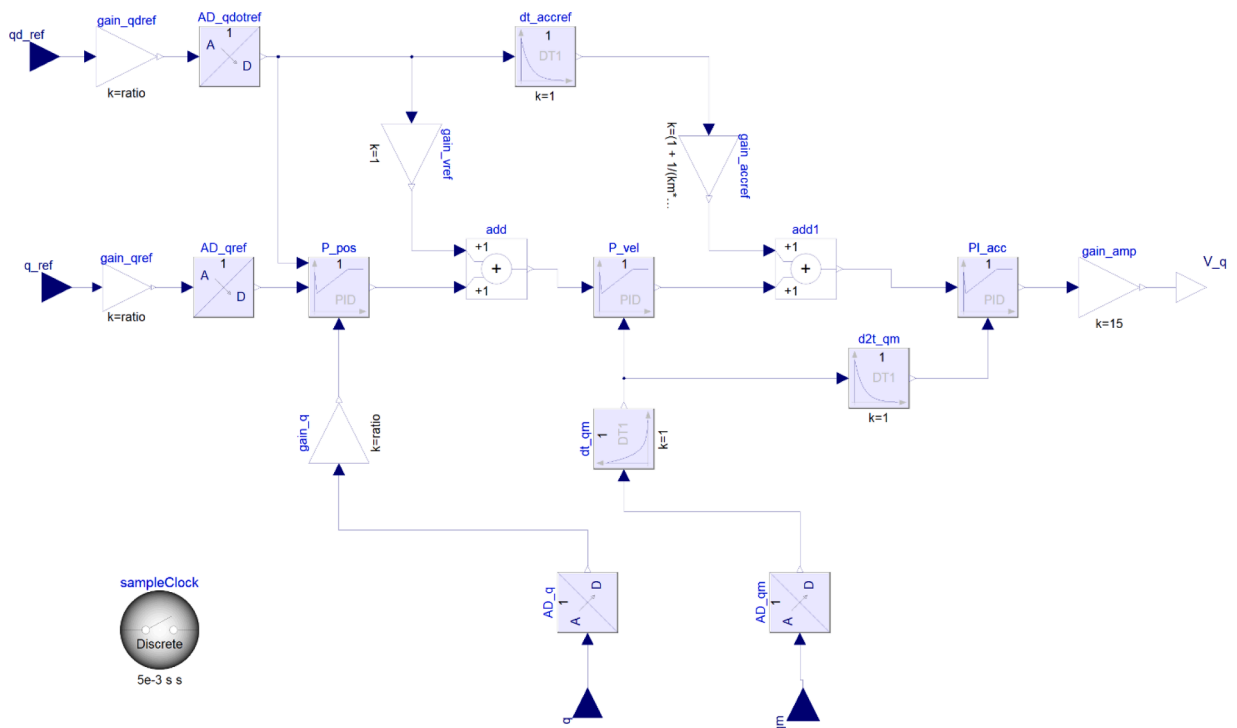


Fig. 15. Block scheme of the PKM motion controller.

Table 7

Notation and parameters of the PKM motion controller.

Block	Description	Specifics/expression
q_{d_ref}	Commanded actuator velocity	Input
q_{ref}	Commanded actuator position	Input
q	Actual actuator position	Input
q_m	Actual motor position	Input
$gain_qdref$	Gain of commanded actuator velocity	25132.74
$gain_qref$	Gain of commanded actuator position	25132.74
$gain_q$	Gain of actual actuator position	25132.74 (laser sensor feedback) 20 (screw encoder feedback) Ideal (no quantization)
AD_qdref	Analog-Digital conversion of commanded actuator velocity	Ideal (no quantization)
AD_qref	Analog-Digital conversion of commanded actuator position	Ideal (no quantization)
AD_q	Analog-Digital conversion of actual actuator position	Resolution 0.01 mm (laser sensor feedback) 0.0055° (screw encoder feedback)
AD_q_m	Analog-Digital conversion of actual motor position	Resolution 0.0055°
$gain_vref$	Gain of velocity feedforward action	1
$gain_accfref$	Gain of acceleration feedforward action	6
$gain_amp$	Amplifier gain	15
dt_q_m	Discrete-time filtered derivative of motor position	10^{-3} (time constant of filtered derivative)
$d2t_q_m$	Discrete-time filtered derivative of motor speed	10^{-3} (time constant of filtered derivative)
$dt_accfref$	Discrete-time filtered derivative of commanded speed	10^{-3} (time constant of filtered derivative)
P_pos	Proportional block of position error	9.615
P_vel	Proportional block of velocity error	390
PI_acc	Proportional-Integral block of acceleration error	$100/s + 100$
V_q	Motor q-voltage control action	Output

Table 8

Loop gain and phase margins.

Parameter	Ideal continuous-time control	5 ms discrete-time control
Gain margin (@ frequency)	21.1 dB (283 rad/s)	11.1 dB (143 rad/s)
Phase margin (@ frequency)	40.8 ° (65.2 rad/s)	31.5 ° (65.2 rad/s)

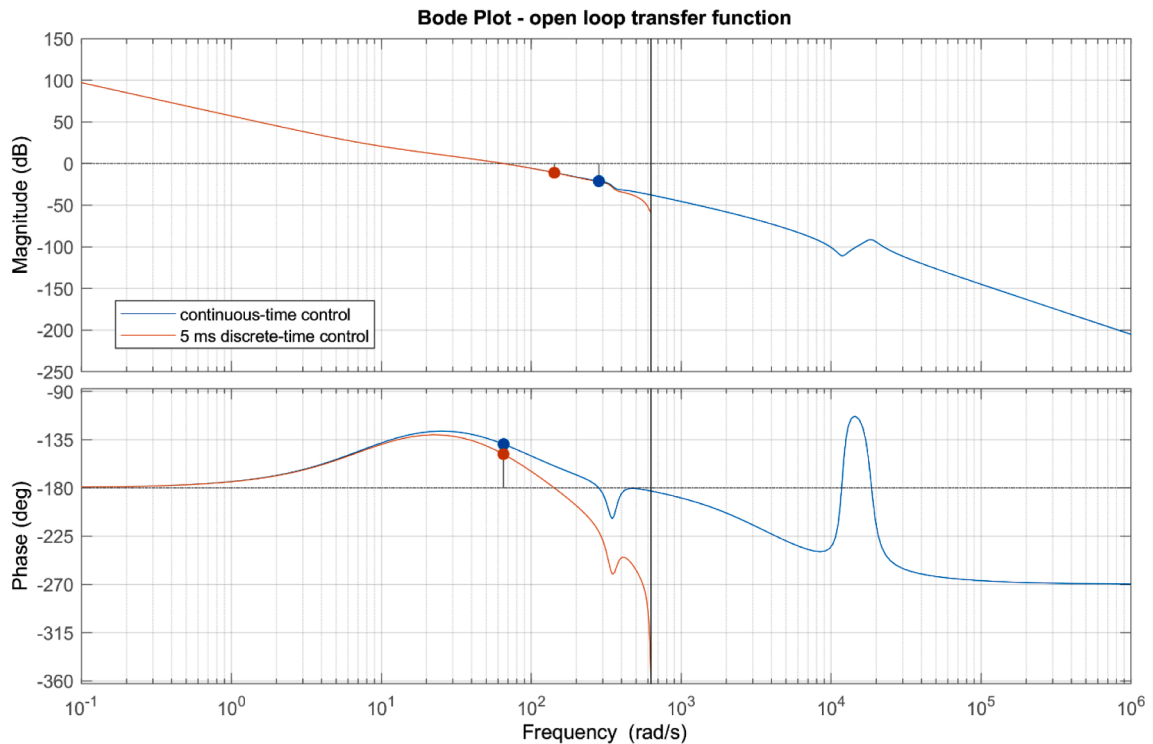
Screw nut. The *screwNut* component, based on the *IdealGearR2T* mechanical component of the Modelica Standard Library, is employed to model the nut of the ballscrew. The model consists in an ideal inertia-less gearbox which transforms a 1-D rotational motion in a 1-D translational one. Employed parameters are shown in Table 6.

3.2. PKM simulator

The PKM device model described in Section 3.1 is used to reproduce the physical behavior of the robot. The full PKM simulator includes a number of additional modules (see Fig. 13) which are here briefly described.

3.2.1. Trajectory generation module

The *trajectoryGeneration* component is employed to generate the reference 6D trajectory (3 translational coordinates and 3 Euler angles) of the PKM end effector (i.e., task space trajectories). This reference command is used as input to the control system, which ensures that the end effector executes the desired motion. The user can specify a number of points in 6D space, and the *trajectoryGeneration* module produces the reference trajectory as straight lines in the 6D space between each two consecutive points. The time profile of each segment is specified according to a cycloidal function (Eq. (3)):

**Fig. 16.** Bode plot of the open loop transfer function.

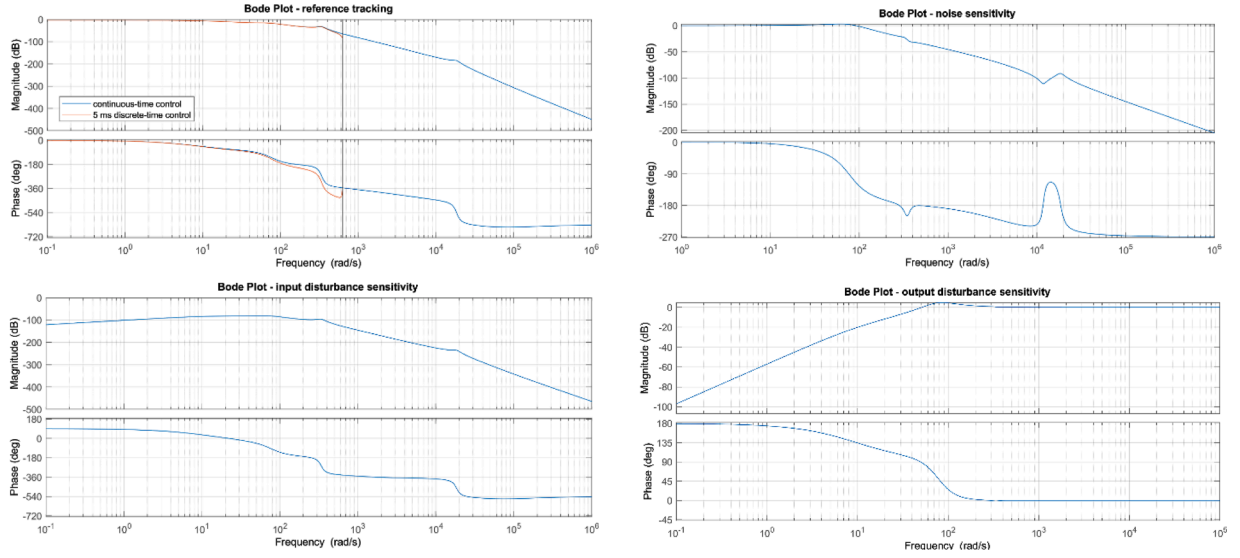


Fig. 17. Bode plots for reference tracking, and noise, input and output sensitivities.

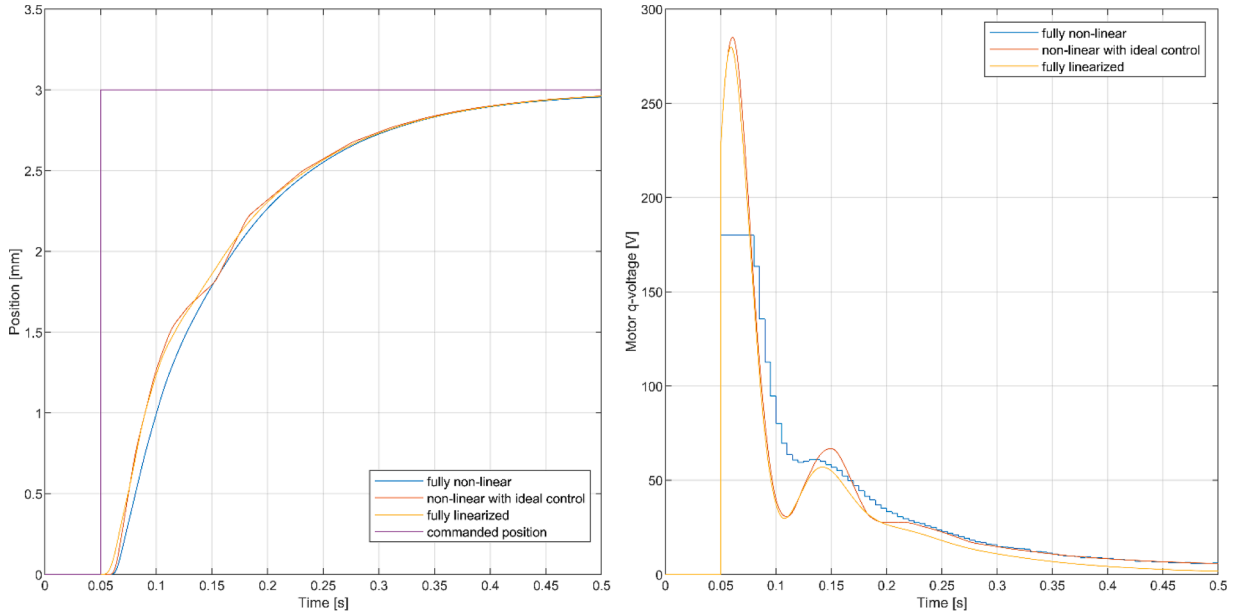


Fig. 18. Response to a 3 mm step change of reference position.

$$\begin{cases} S(t) = S_0 + (S_f - S_0) \left[\frac{t - t_0}{t_f - t_0} - \frac{1}{2\pi} \sin \left(2\pi \frac{t - t_0}{t_f - t_0} \right) \right] \\ \dot{S}(t) = (S_f - S_0) \frac{1}{t_f - t_0} \left[1 - \cos \left(2\pi \frac{t - t_0}{t_f - t_0} \right) \right] \\ \ddot{S}(t) = (S_f - S_0) \frac{2\pi}{(t_f - t_0)^2} \sin \left(2\pi \frac{t - t_0}{t_f - t_0} \right) \end{cases} \quad (3)$$

Where subscripts 0 and f stand for starting and final, and the S is the Mobile Platform pose vector:

$$S = (x_C \ y_C \ z_C \ \theta \ \varphi \ \phi)^T$$

Cycloidal⁶ reference trajectories have been selected because they have continuous derivatives up to any order – i.e., they do not have jumps in velocity, acceleration, jerk, or any higher order derivatives. The user can specify as parameters the maximum allowable value of velocity, acceleration and jerk, and the *trajectoryGeneration* module computes the motion execution time and the reference trajectory, assuming a complete stop at each point. The *trajectoryGeneration* module produces task-space trajectories. The conversion from task-space trajectories to the corresponding joint-space ones is deputed to the

⁶ Cycloidal trajectories present the major drawback of being highly time-inefficient. However, due to the working condition of the PKM (small motions at small velocities), this does not constitute a significant problem. Priority is given to the advantage of motion smoothness and of preventing any jerky motion of the robot, given the large payload and the required high resolution.

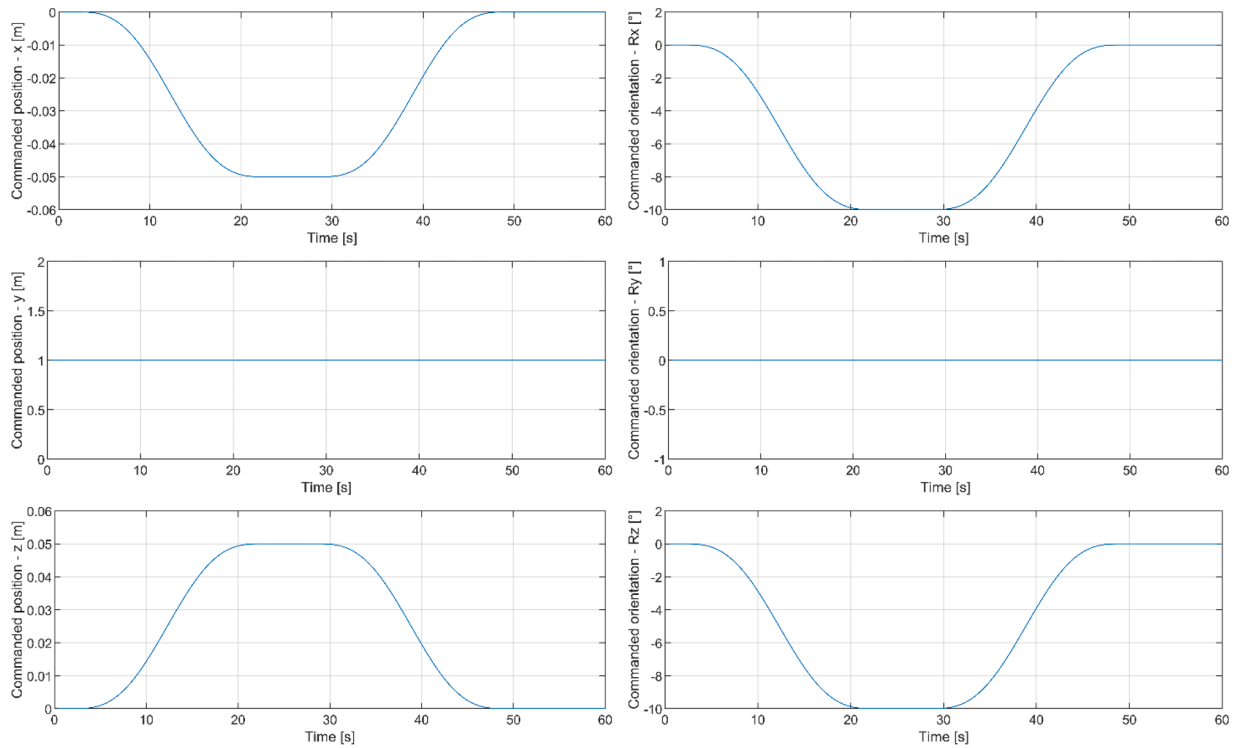


Fig. 19. Commanded position (left) and orientation (right).

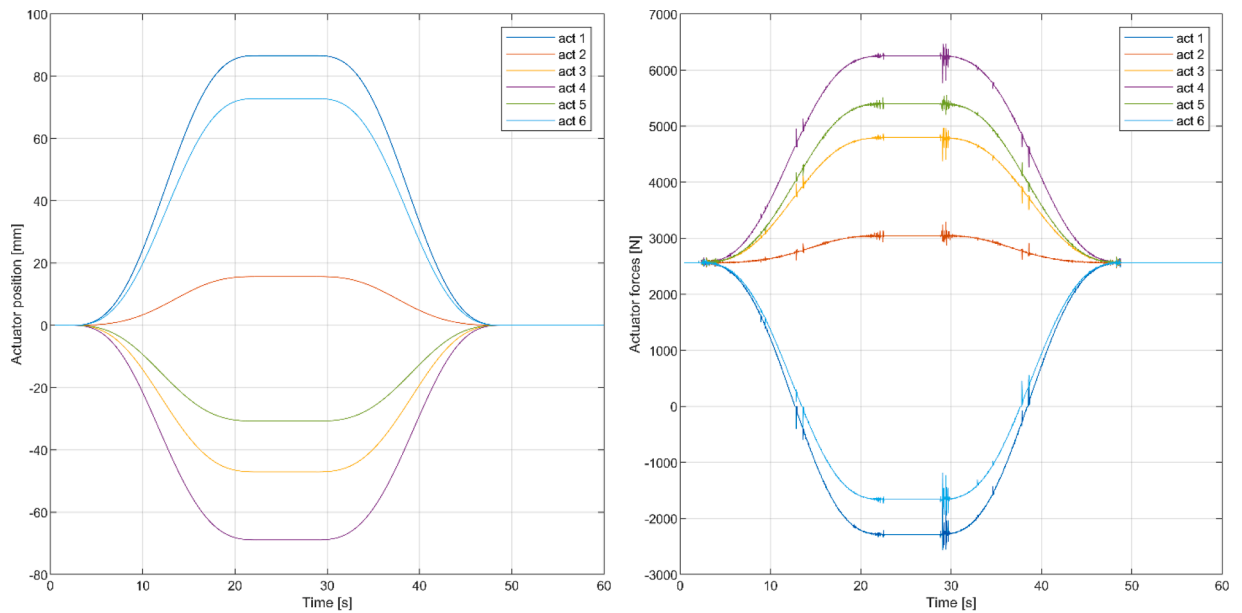


Fig. 20. Actuators positions (left) and forces (right).

Modeling module described in [Section 3.2.4](#).

3.2.2. Input/output module

The *inputOutput* component constitutes the interface between the *servoBus* connector ([Section 3.1.4](#)) – employed for multiplexing and managing the field signals to/from the PKM device – and the *controlBus* connector ([Section 3.2.5](#)). It is a simple component merely used for multiplexing and signals ordering/housekeeping.

3.2.3. Motion controller

The motion controller module is deputed to the implementation of

the PKM motion control algorithms – i.e., the generation of the motors power signals required for the execution of the end-effector desired motion. It is described in more detail in [Section 4](#).

3.2.4. Kinematics and dynamics modeling module

The Kinematics and Dynamics Modeling module is an ad-hoc component created for performing all the computations required for robot control and state estimation. Robot's Inverse Kinematics ([Eq. \(4\)](#)) is used to transform the commanded trajectory from task space (end-effector Cartesian position and orientation) to joint space (legs lengths or, equivalently, motors positions). In [Eq. \(4\)](#), \bar{R} is the rotation matrix of

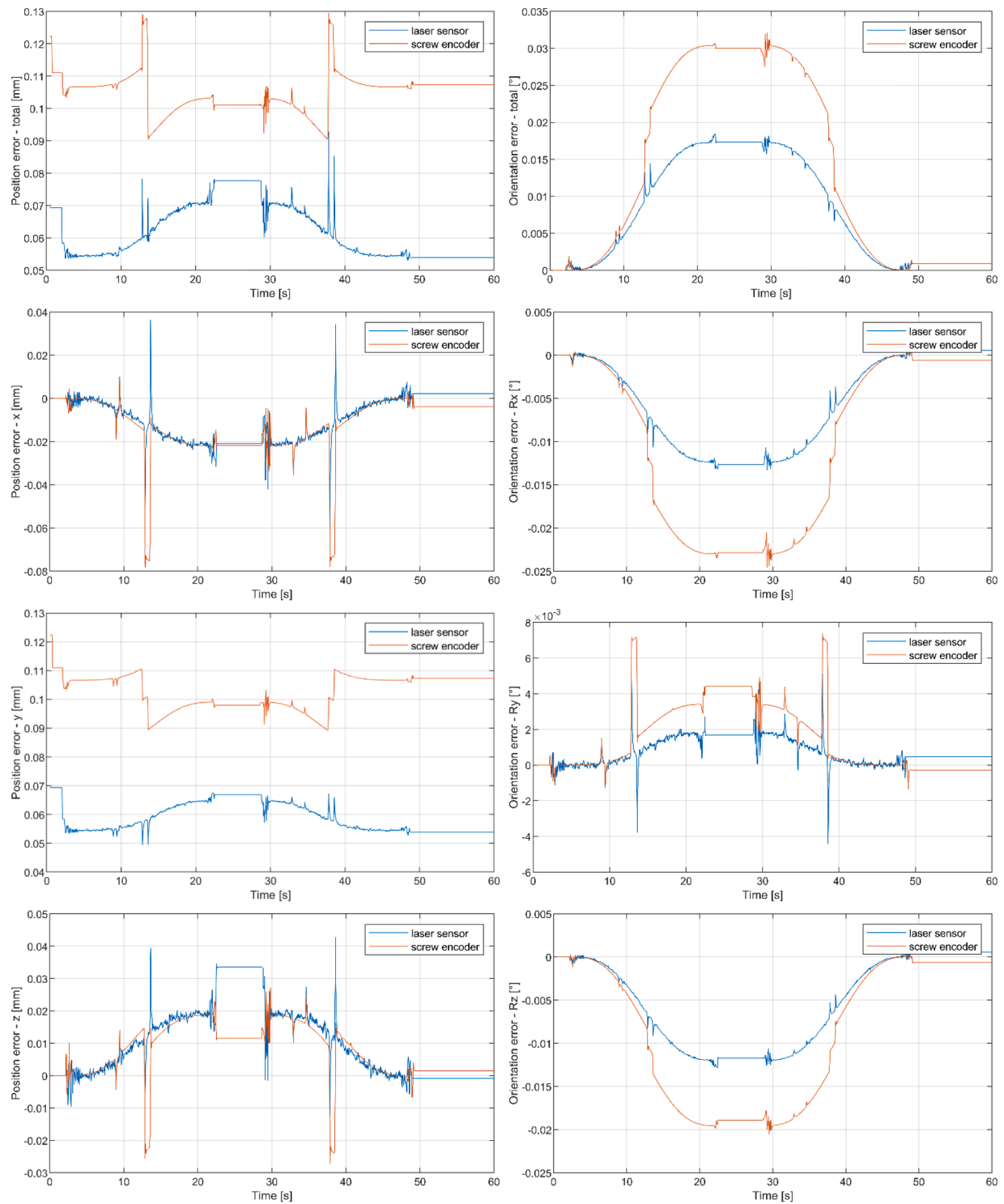


Fig. 21. Position (left) and orientation (right) errors.

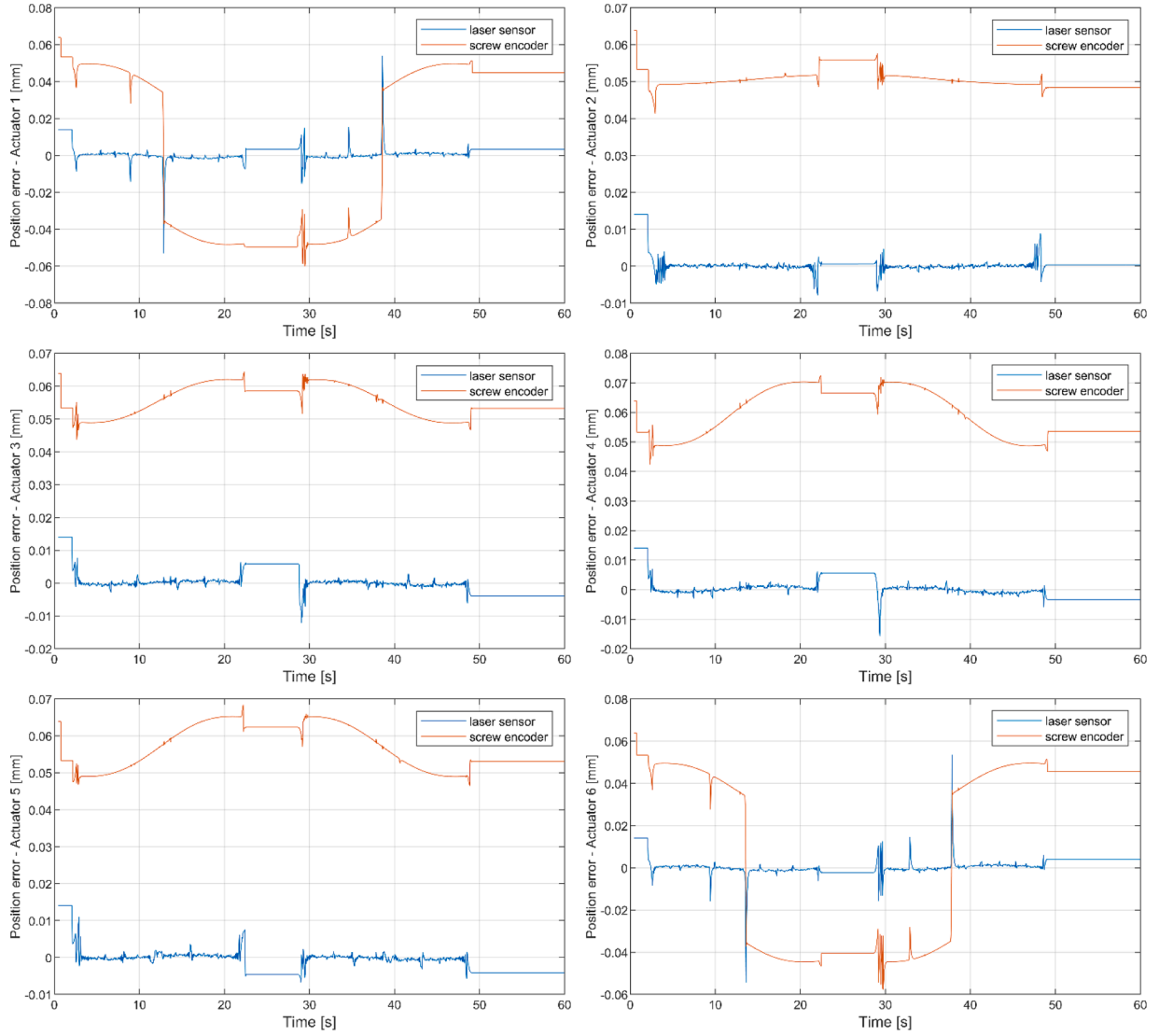


Fig. 22. Actuators errors.

the Mobile Platform, q is the joint-space coordinate vector, c_i and s_i indicate sine and cosine, respectively, and the notation is that shown in Fig. 4. The commanded actuators positions are used as reference input for joint-space motion control, as will be described in Section 4.

$$b_i t_i = OC + \bar{R}^T \cdot C t_i - Ob_i$$

$$\bar{R} = \begin{bmatrix} c_\phi c_\varphi & c_\phi s_\varphi s_\beta + s_\phi c_\beta & -c_\phi s_\varphi c_\beta + s_\phi s_\beta \\ -s_\phi c_\varphi & -s_\phi s_\varphi s_\beta + c_\phi c_\beta & s_\phi s_\varphi c_\beta + c_\phi s_\beta \\ s_\varphi & -c_\varphi s_\beta & c_\varphi c_\beta \end{bmatrix}$$

$$q = \begin{pmatrix} |b_1 t_1| \\ \vdots \\ |b_6 t_6| \end{pmatrix} \quad (4)$$

The Modeling module also implements the robot's Kinematic Jacobian matrix \bar{J}_k – needed for conversion of forces, moments and velocities between task and joint spaces –, whose inverse can be computed as Eq. (5) [5]:

$$\bar{J}_k^{-1} = \begin{pmatrix} \frac{b_1 t_1^T}{|b_1 t_1|} & \left(\bar{R} \cdot C t_1 \times \frac{b_1 t_1}{|b_1 t_1|} \right)^T \\ \vdots & \vdots \\ \frac{b_6 t_6^T}{|b_6 t_6|} & \left(\bar{R} \cdot C t_6 \times \frac{b_6 t_6}{|b_6 t_6|} \right)^T \end{pmatrix} \quad (5)$$

The theoretical actuators forces τ_i can be computed as in Eq. (6):

$$\begin{cases} \tau = \bar{J}_k^T W \\ W = (F M)^T \\ \tau = (\tau_1 \dots \tau_6)^T \end{cases} \quad (6)$$

Where $F = (F_x, F_y, F_z)^T$ and $M = (M_x, M_y, M_z)^T$ are, respectively, the force and moment acting on the Platform, calculated with respect to the Platform reference point C , and the inversion of \bar{J}_k^{-1} has to be performed numerically. The theoretical actuators forces τ_i , computed along the reference trajectories, can be used for contact detection and resolution or to implement computed-torque-based motion control algorithms [29]. In the scope of this paper, the theoretical forces are used for model verification and to estimate the different contributions to the resulting actuators forces. In particular, it is possible to discriminate between gravitational terms (Eq. (7)), inertial terms (Eq. (8)) and Coriolis/centrifugal terms (Eq. (9)):

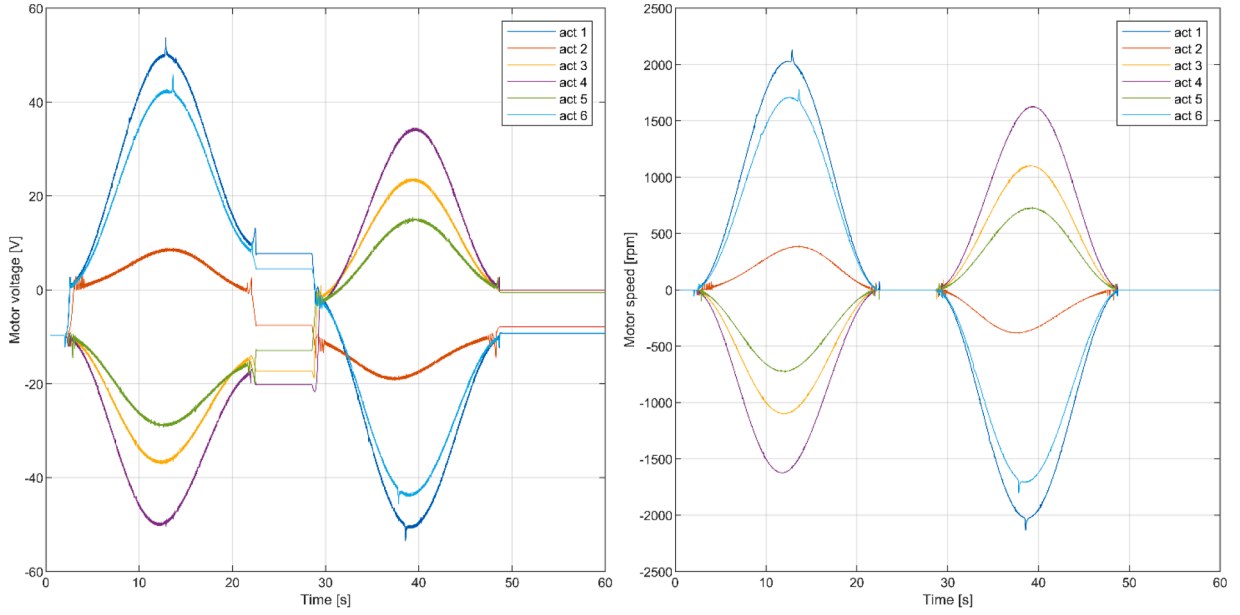


Fig. 23. Motor voltages (left) and speeds (right).

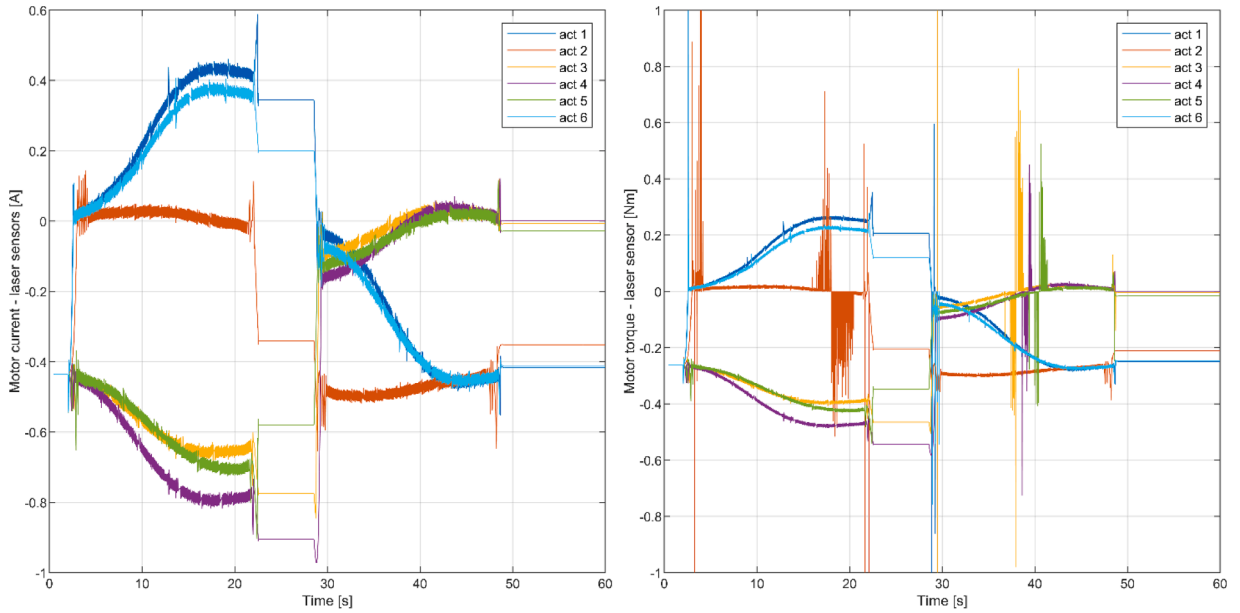


Fig. 24. Motor currents (left) and torques (right) for laser sensor position feedback.

$$\tau_{grav} = \bar{J}_k^T \begin{pmatrix} mg \\ -mGC \times g \end{pmatrix} \quad (7)$$

$$\tau_{iner} = \bar{J}_k^T \begin{pmatrix} m\ddot{\bar{I}}_3 & mGC \\ -mGC & \bar{I} - mGC^2 \end{pmatrix} \begin{pmatrix} \dot{V} \\ \dot{\Omega} \end{pmatrix} \quad (8)$$

$$\tau_{centr} = \bar{J}_k^T \begin{pmatrix} m\omega \\ \Omega \times \bar{I}\Omega + mGC \times \omega \end{pmatrix} \quad (9)$$

Where m , \bar{I} and GC are, respectively, the total (platform body plus payload) mass, inertia tensor and center of mass vector with respect to platform reference point C , V and Ω are the platform translational and rotational velocities, $\omega = (\Omega \times GC) \times \Omega$, and g is the gravity vector. In Section 5 it will be shown how, for the operating conditions of the PKM, the latter two terms are negligible with respect to the gravitational one.

3.2.5. Control bus

The *controlBus* component is a Modelica connector employed for signal multiplexing, i.e. to communicate input/output signals from/to the PKM device.

4. PKM motion control

The motion control problem consists in determining the time history of the motors input signals (voltages or currents) required for the execution of the commanded end-effector trajectory, satisfying at the same time certain transient and steady-state requirements.

As the commanded trajectories are specified in task space as end-effector position and orientation, the trajectories must be firstly mapped to joint space. In other words, it must be determined the motors positions required for the execution of the desired trajectories. These commanded joint-positions are then used as reference input for the

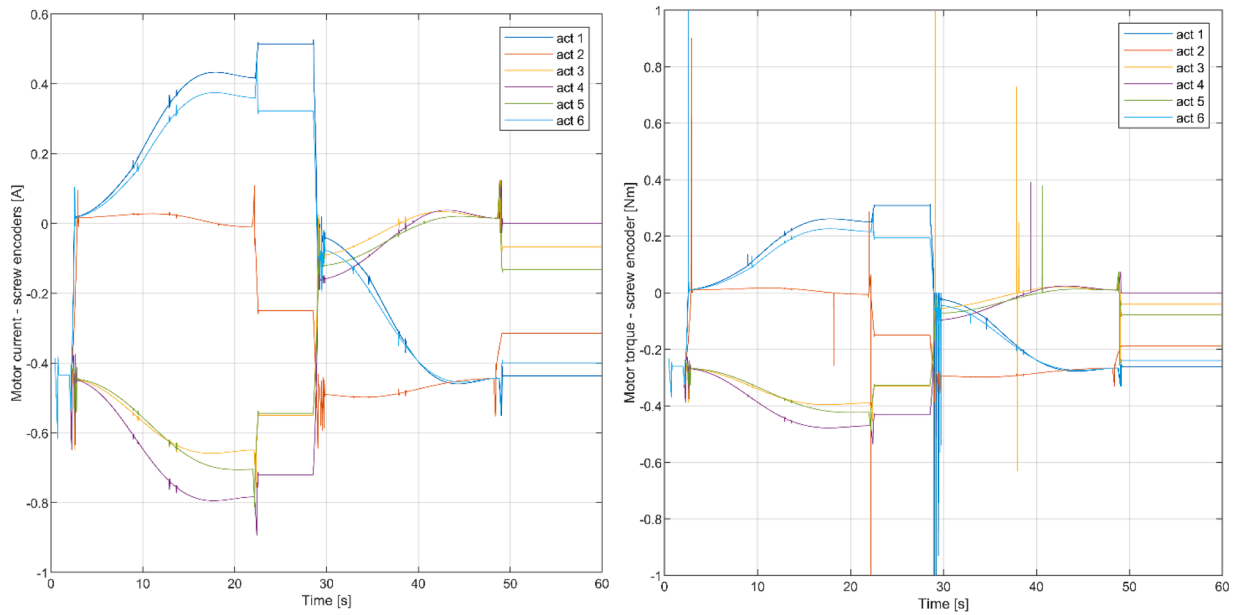


Fig. 25. Motor currents (left) and torques (right) for screw encoder position feedback.

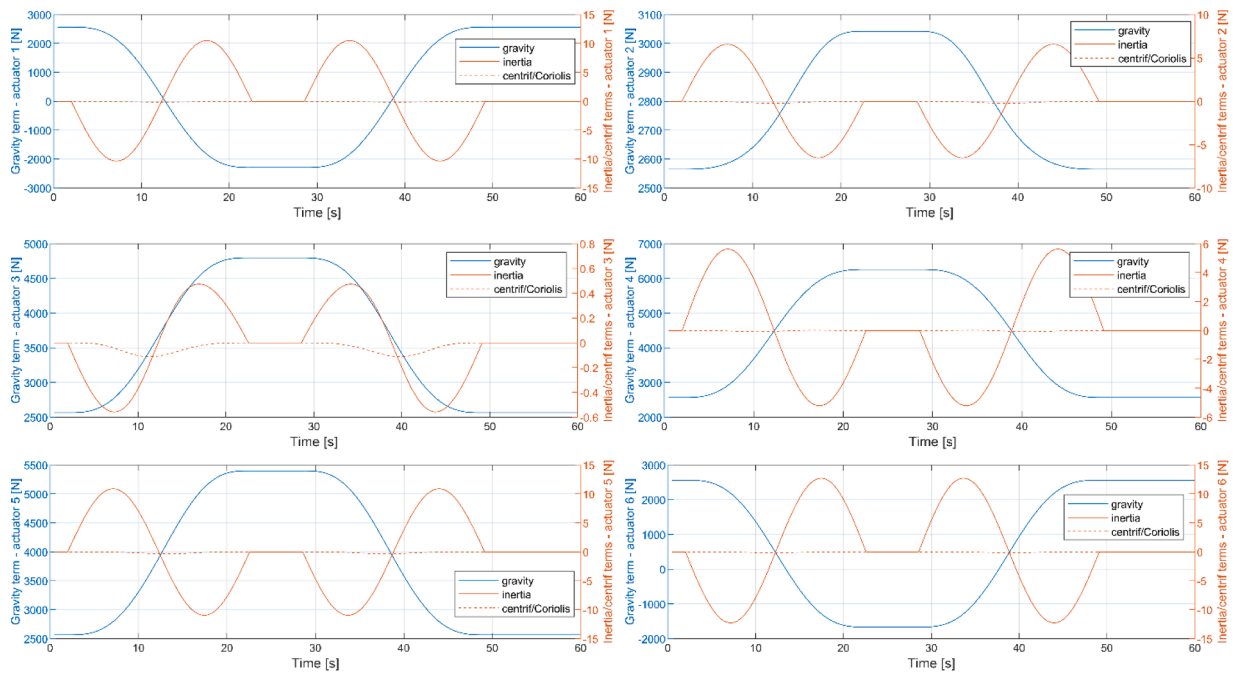


Fig. 26. Breakdown of calculated actuators force terms.

control system. This approach is the base of the so-called joint-space control (Fig. 14). The Inverse Kinematics transformation is performed by the Modeling module (Section 3.2.4). This Section describes the design of the motion controller that ensures that the actual joint motion q tracks the reference joint motion q_{ref} .

The working conditions of the PKM are characterized by very limited dynamical requirements and large gear-reduction ratios. In this situation, the non-linear and coupled terms of the manipulator dynamics are either of very small magnitude (inertial and centrifugal/Coriolis terms) or are very slowly-varying (gravitational term). This allows the adoption of so-called “decentralized” (also known as “independent-joints”) control schemes [30], in which the robot is considered composed of n independent joints, each to be independently controlled as a SISO (Single-Input-Single-Output) system where the coupled terms are

treated as disturbances to be rejected by the control algorithm⁷. The main advantage of the independent-joint approach is the strong reduction of the computational burden on the motion controller⁸, allowing to achieve higher control cycle rates and thus stricter control, higher resolution and higher disturbance rejection.

The limited velocities and large transmission ratios also allow

⁷ Other disturbances, the main of which is static friction in gears, bearings, etc., are intrinsically single-joint in nature.

⁸ In particular, the robot Forward Kinematics does not enter in the control loop. This constitutes a significant advantage, as for the Stewart-Platform-like 6-DoF parallel robots the Forward Kinematics involves iterative algorithms for a non-closed, multiple-solutions problem.

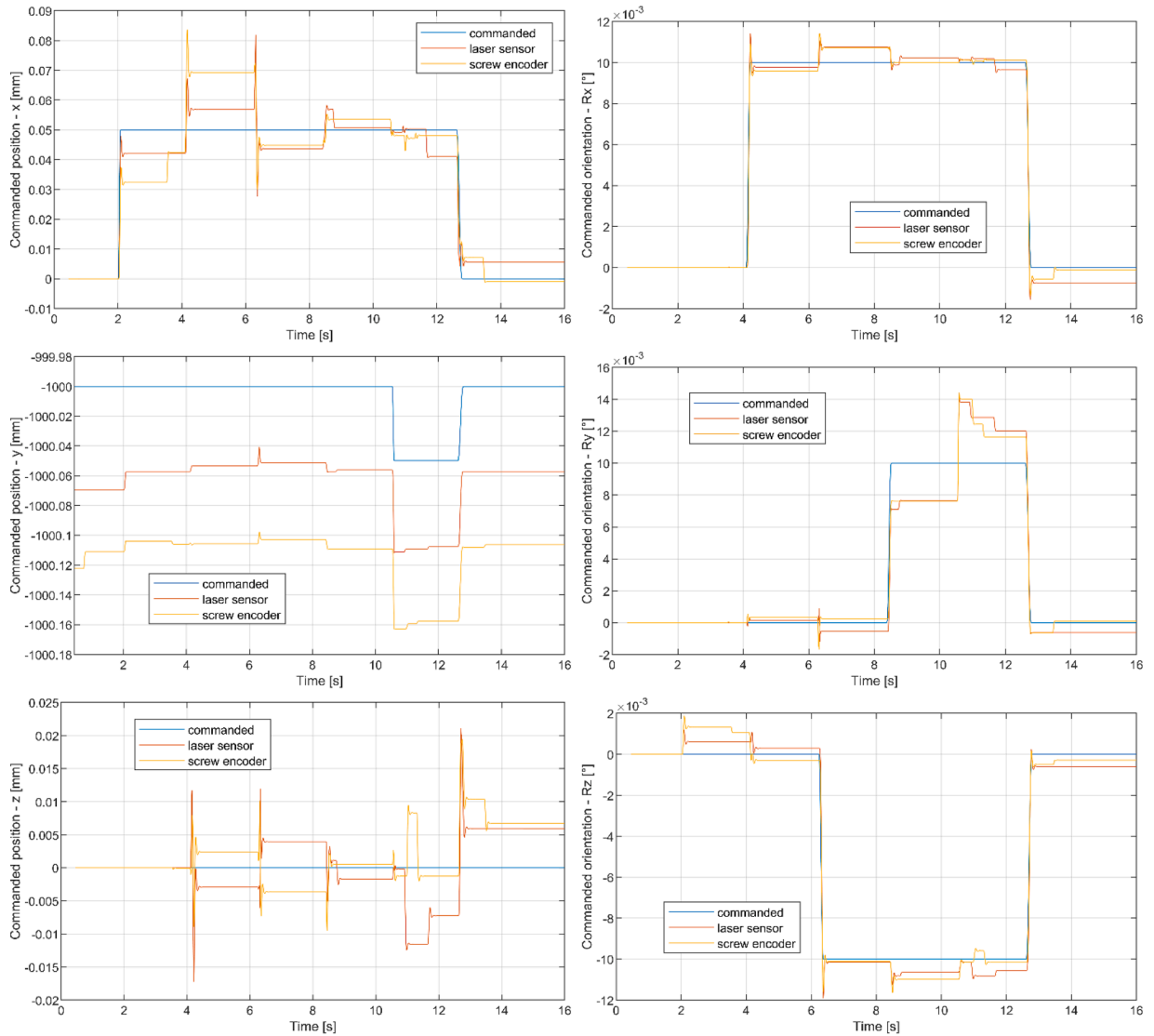


Fig. 27. Reference and actual position (left) and orientation (right) for laser sensor and screw encoder position feedback, for the fine motion simulation.

operating the motors as voltage-controlled devices, i.e., to consider the motor velocities to be approximately proportional to the motor voltages [30], independently on the exact values of manipulator parameters. This confers a degree of inherent robustness to the control system with respect to parameters variation or lack of model knowledge.

The block scheme of the control algorithm, identical for each of the six independent joints, is shown in Fig. 15. It consists of a cascade-PID (Proportional-Integral-Derivative) control scheme with dual motor-and-load feedback and with velocity and acceleration feedforward. The control system is implemented in the same Dymola environment, and it makes use of the *Modelica_LinearSystems2* library [26] for the implementation of digital control. Meaning of the symbols and parameters' values are reported in Table 7. Note that the motor amplifiers are modeled as a simple gain, i.e., they are modeled as ideal components, neglecting the internal electronics dynamics.

The cascade-PID configuration, which is equivalent to a 2-DoF PID controller [30], has been chosen due to the possibility to introduce a conditional dead zone in the outer position feedback loop (P_{pos}). It produces a zero output when the position error lies inside a user-specified dead zone, and it is activated only when the reference joint velocity is zero. It is used to prevent actuator hunting due to the significant static friction.

The so-called dual-loop control [31], i.e., with separated feedbacks

from motor and load sensors, is nowadays an industry standard for compensation of backlashes, compliances and elasticities in applications requiring high positioning accuracy⁹ and resolution. It consists in an outer position control loop with feedback from a load-installed position sensor, and an inner velocity control loop with feedback from a motor-installed position sensor. The outer loop closes directly on load position, thus it directly compensates for any backlash or deformation in the kinematic chain. The inner loop, on the other hand, closes directly on motor position, thus eliminating any delay in the loop's response time, e.g. due to backlashes and static friction, improving the dynamic performances and stability of the control system.

Two different options are considered for load-side position feedback. The first consists in a 16-bit absolute encoder installed on the ballscrew body, the second consists in a laser distance sensor installed on the actuator body. There are tradeoffs to consider in the selection of the load-side sensor: the ballscrew encoder offers a much higher resolution, but it cannot compensate for the downstream backlash and deformation;

⁹ It should be noted that the accuracy requirement is not a stringent one for the PKM, as the robot operates in an unstructured environment and end-effector's final adjustments will be performed under operator manual control with visual feedback.

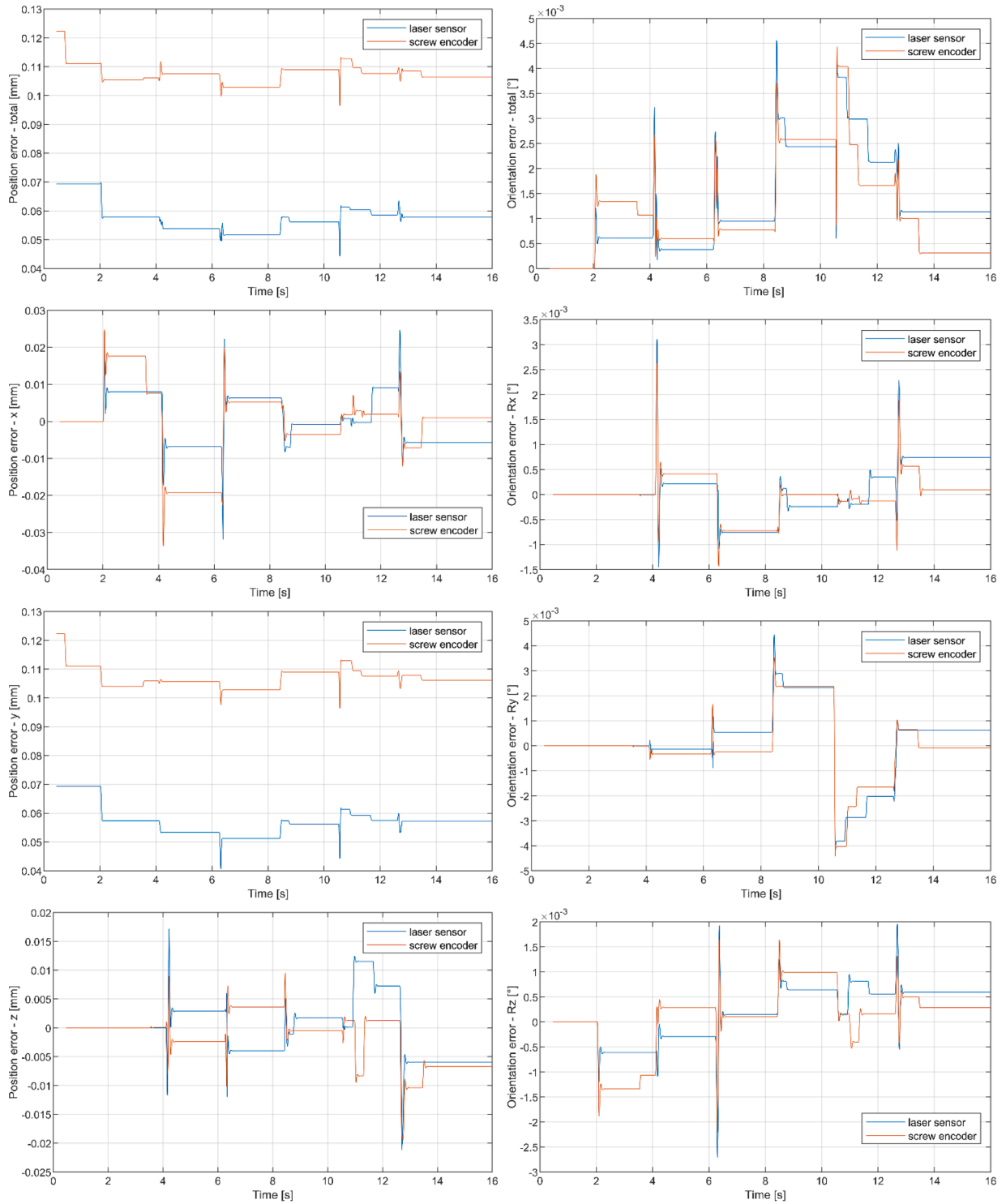


Fig. 28. Position (left) and orientation (right) errors.

the laser sensor can directly measure the actual actuator position, but its resolution is significantly lower. In Section 5, simulations are conducted for both configurations.

The EMA model (Section 3.1.5) includes the nonlinearities caused by the backlashes between components and the friction characteristics of the gears and bearings. For control system design and tuning, the corresponding linearized EMA model has been implemented by removing backlashes and substituting the friction characteristics with linear approximations. The Dymola simulation environment allows the export of the Linear-Time-Invariant (LTI) system in matrix form. This can easily be

imported in control design toolboxes (e.g. the Matlab Control Toolbox [32]), where conventional LTI-analysis techniques can be used.

Fig. 16 shows the Bode Plot of the open loop transfer function of the linearized EMA model under the control scheme shown in Fig. 15, for both ideal continuous-time control and discrete-time control with a 5 milliseconds cycle time. Gain and phase margins are reported in Table 8. It can be clearly seen how the control frequency has a significant impact on the phase and, in particular, the gain margin of the loop transfer function. Control frequency is limited by the data bandwidth of the multiplexed communication that is required for PKM operation (see

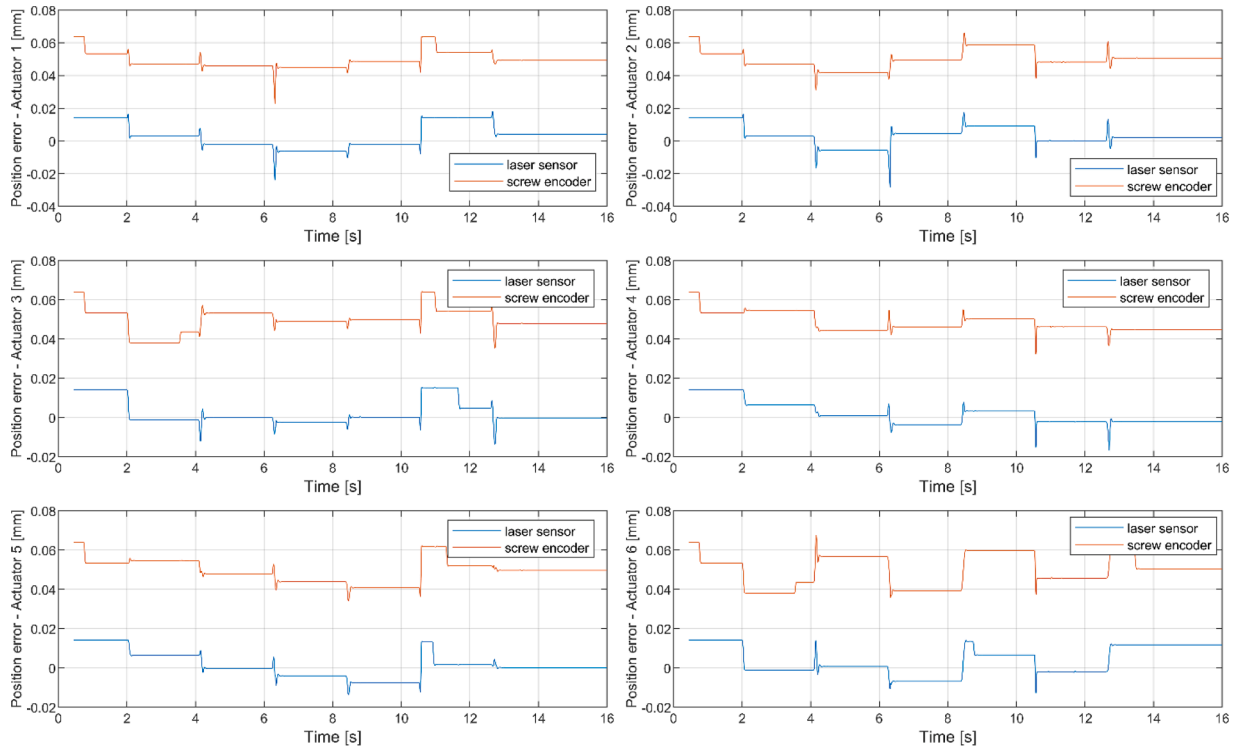


Fig. 29. Actuators errors.

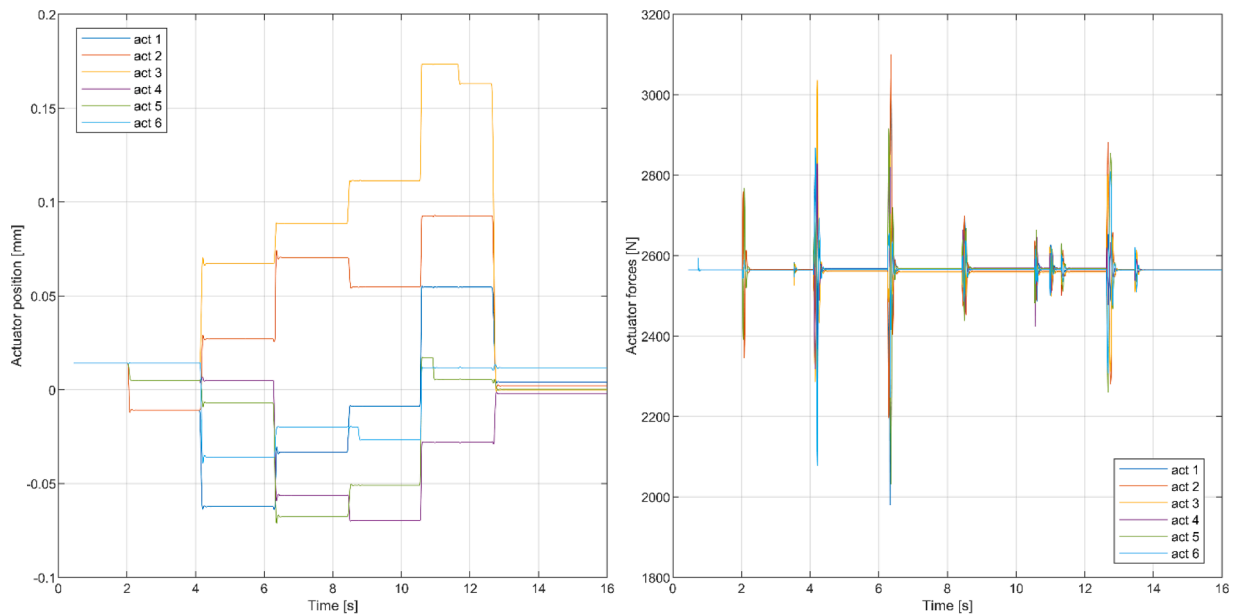


Fig. 30. Actuators positions (left) and forces (right).

Section 2). Fig. 17 shows the Bode plots of the reference tracking and of the noise, input and output sensitivities.

Fig. 18 shows the response of the controlled EMA to a 3.0 millimeters step change in the commanded position, without the feedforward control action, for three different system configurations:

- i The fully non-linear system, i.e. non-linear EMA model with control scheme shown in Fig. 15 and Table 7;
- ii The non-linear EMA model with ideal control, i.e. continuous-time control with no quantization errors (i.e. with sensors infinite resolution) and no amplifier saturation;

- iii The fully linearized system, i.e. linearized EMA with ideal control described in point II;

From Fig. 18 it can be noticed how time delays are introduced in the response of the system both due to the EMA nonlinearities (backlashes and static friction) and to the control nonlinearities (saturation and discrete-time) action.

5. Simulations and results

The PKM simulator described in Section 3 is here used to investigate

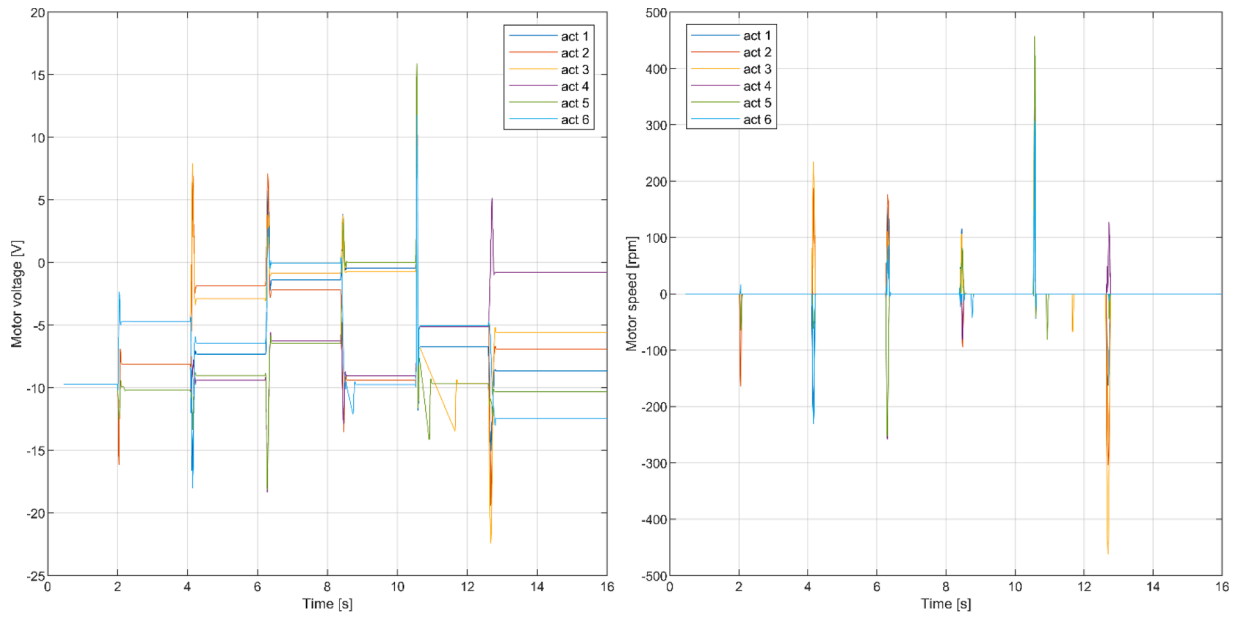


Fig. 31. Motors voltages (left) and speeds (right).

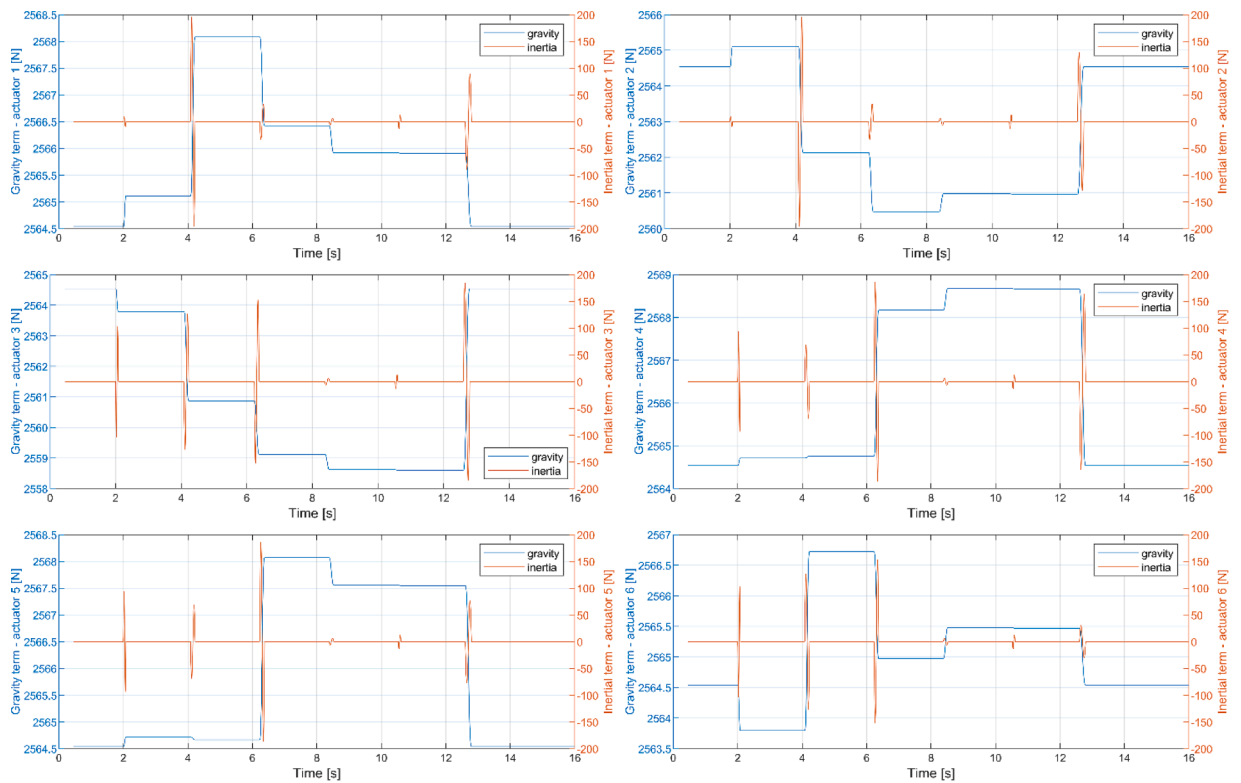


Fig. 32. Breakdown of calculated actuators force terms.

the performance of the robot, and, in particular, the effectiveness of the control strategy developed in Section 4 and the impact that backlashes and static friction have on robot resolution, accuracy, repeatability and joints stresses. Two different robot motions are simulated:

- i An ample motion, with the main focus of assessing the effect that backlashes have on robot accuracy over a wide range of Platform poses (i.e., a wide range of forces acting on the actuators, mainly due to the gravitational terms);

- ii A fine motion, with the main focus of assessing robot's achievable position and orientation resolutions.

The commanded point-to-point trajectories shapes are those described in Section 3.2.1. For both the motions, two different options are considered for the sensors providing load-side position feedback (see Section 3.1.5): a laser distance sensor (with a resolution of 0.01 mm) directly installed on the actuator, and a 16-bit encoder (with a resolution of 0.0055°) installed on the screw spindle.

5.1. Large motion

For the large motion simulation, the commanded effector trajectory is shown in Fig. 19, where the time evolution of the different components (positions and orientations) is provided. Fig. 20 shows the actual actuators positions¹⁰ and the measured actuators forces. Maximum forces on the actuators are crucial variables, as they determine the sizing of actuators' components, and thus in the end PKM's proper weight. It can be clearly seen a degree of jerkiness in the forces at the initial and final portions of the motions and when the stress change from tension to compression. These effects are due to combined actions of backlashes and static friction.

Fig. 21 shows the evolution of the Platform's positioning and orientation errors (both the total errors and the breakdown for the individual components x , y , z , R_x , R_y , R_z), while Fig. 22 shows the evolution of the position errors for each of the six actuators. The latter clearly shows how the adoption of screw-encoder position feedback produces: (i) larger steady actuators errors due to the uncompensated elasticities and backlashes downstream of the sensor in the kinematic chain; and (ii) how operation around zones where forces undergo transitions between tension and compression (actuators 1 and 6) present sudden jumps in the errors due to backlashes. These effects are clearly reflected in the Platform pose errors (Fig. 21), where: effect (i) translates in a larger error in y -direction, and effect (ii) produces large jumps in particular in orientation errors.

Fig. 23 shows the motors q -voltages and the motors velocities, with reference to the laser-sensor feedback configuration¹¹. As highlighted before, a somewhat jerky behavior appears in the initial acceleration and final deceleration phases, mainly due to static friction.

Figs. 24 and 25 show the time history of motors currents and torques, respectively for laser-sensor and screw-encoder configurations. A comparison between the figures shows that the worse resolution of the laser sensor causes a less smooth behavior of the motors currents – and therefore torques – due to the less smooth control action. This effect shall be carefully analyzed for the possibility of exciting system's proper frequencies of un-modeled dynamics.

Fig. 26 shows the breakdown of the actuators forces between the gravitational, inertial and centrifugal/Coriolis terms, computed as described in Section 3.2.4. It can be seen how, for the considered robot trajectory, the latter two terms are negligible with respect to the gravitational one. In addition, the computed force values in Fig. 26 show excellent agreement with those obtained by the simulation of the PKM device model shown in Fig. 20.

5.2. Fine motion

The second simulation analyzed is constituted by fine adjustments ($50\text{ }\mu\text{m}$ and 0.01°) of the Platform pose. The commanded and actual trajectory profile is shown in Fig. 27, while Fig. 28 shows the positioning and orientation errors. The actuators errors are shown in Fig. 29. Besides the steady actuators errors caused by uncompensated elasticity (which, as for the previous simulation, are larger for the screw-encoder configuration) which are reflected in a loss of accuracy particularly in the y -direction, the robot shows excellent resolution, indicating the effectiveness of the control system in rejecting friction disturbances¹². Of course, for the screw-encoder configuration, the resolution would be severely affected when operating near points of transition between

tension and compression, as described in Section 5.1.

Fig. 30 shows the evolution of actuators positions and forces, while Fig. 31 show the motors voltages and speeds, both with reference to the laser-sensor configuration (results for the screw-encoder configuration are similar). The breakdown between the gravitational and inertial force terms is shown in Fig. 32 (centrifugal and Coriolis terms are essentially zero). Note how the inertial terms are much larger for the fine motion scenario than for the large motion one. This is due to the features of the cycloidal trajectories: for ample motions they tend to be velocity-limited (while acceleration and jerk are much lower than their maximum allowable values), whereas for smaller motions they tend to be acceleration-limited, with resulting higher inertial term. The discrepancies, in the peaks of the forces, between simulated (Fig. 26) and calculated (Fig. 32) values are due to the effects of backlashes and static friction.

6. Conclusions

This paper describes the modeling and simulation activities performed, within the framework of the EUROfusion Consortium, in support to the engineering design and the control system design of the DONES PKM, a robotic device part of the Remote Handling System of the DONES facility. The PKM is a 6-DoF parallel robot based on the Stewart platform design. A control-oriented dynamics simulator has been developed by employing validated libraries of the object-oriented Modelica language. The PKM model is able to reproduce the dynamics of the robot, with particular attention on realistic modeling of the behavior of the electro-mechanical linear actuator. The model includes the main nonlinearities constituted by the backlashes in the couplings between components and the static friction in gears and bearings. Friction, in particular, is implemented in a physically meaningful way, reproducing the Stribeck friction curve and accounting for locking of the movements (of gears and bearings) at zero speed due to static friction. Backlashes and static friction are crucial phenomena for the impact they have on the achievable robot performances and on the definition of control algorithms. The PKM simulator also includes a module for trajectory generation, a module performing all required computations (e.g., inverse kinematics, etc.), a module reproducing the motion controller, and all required signals multiplexing and input/output.

The PKM simulator is then used to support the development of the robot control system. A preliminary PKM control system is designed, based on an independent-joint approach and adopting a cascade-PID logic with dual (motor and load) feedback for actuators position. Two options are explored for the load-side position feedback: a standard encoder installed on actuators' screws, and a laser sensor installed on actuators bodies. Tradeoffs between the two options are analyzed and discussed based on simulations results. The adoption of the laser sensor provides a better accuracy, as it allows to compensate for elastic deformation and backlashes of the actuator. On the contrary, adopting the screw encoder ensures a smoother behavior in terms of motors currents and torques, thanks to the higher intrinsic resolution of this sensor with respect to the laser one.

The PKM simulator is then used to obtain a first assessment of the achievable performances of the robot in terms of resolution, accuracy and repeatability, as well as indications on generated forces on PKM components. Preliminary indications from simulations outcomes show a level of performances in line with design requirements. The accuracy and repeatability are significantly better than the respective required values (0.5 mm for translation and 0.1° for orientation): for screw encoder feedback, translation and orientation errors are about 0.13 mm and 0.03° , respectively; for laser sensor feedback, the values are about 0.08 mm and 0.02° . Regarding the resolution, both sensors options ensure a performance in line with the requirement (0.05 mm for translation and 0.01° for orientation). The decentralized independent-joint control logics with dual-feedback cascade-PID algorithm is confirmed, despite its conceptual simplicity, to provide satisfying performances.

¹⁰ Actuators positions are expressed as variations from the reference actuators zeros, which correspond to a leg length of 0.9343 m .

¹¹ The simulations for the screw-encoder configuration do not show visible differences, except those that are highlighted in the following concerning motors currents and torques.

¹² As explained in Note 9, robot's *accuracy* is not a stringent requirement for the PKM. The key figure-of-merit is robot's *resolution*.

This is mainly due to the extremely limited dynamical requirements of the PKM, which ensures that the non-linear and coupled terms of the manipulator dynamics are either of very small magnitude (inertial and centrifugal/Coriolis terms) or are very slowly-varying (gravitational term).

Future work includes model validation activities as well as an improvement of the level of detail of the model, in particular concerning the behavior of the electric motors and amplifiers. In addition, the simulator described in this paper can easily be employed for developing and testing more sophisticated control strategies, e.g. computed-torque-like and inverse-dynamics-based control schemes.

Declaration of Competing Interest

The authors declare that they have no known competing financial interests or personal relationships that could have appeared to influence the work reported in this paper.

Data availability

Data will be made available on request.

Acknowledgements

This work has been carried out within the framework of the EURO-fusion Consortium and has received funding from the Euratom research and training programme 2014-2018 and 2019-2020 under grant agreement No 633053. The view and opinions expressed herein do not necessarily reflect those of the European Commission.

References

- [1] A. Ibarra and, et al., The IFMIF-DONES project: preliminary engineering design, *Nucl. Fusion*. 58 (10) (2018).
- [2] W. Krolas and, et al., The IFMIF-DONES fusion oriented neutron source: evolution of the design, *Nucl. Fusion*. 61 (12) (2021).
- [3] European Strategy Forum on Research Infrastructures, Strategy Report on Research Infrastructures Roadmap 2018, European Strategy Forum on Research Infrastructures, 2018 [Online]. Available: roadmap2018.esfri.eu/.
- [4] K. Tian and, et al., Preliminary analysis on a maintainable test cell concept for IFMIF-DONES, *Fusion Eng. Des.* 146 (2019) 505–509.
- [5] J.P. Merlet, *Parallel Robots*, 2nd ed., Springer, 2006.
- [6] B. Dasgupta, T.S. Mruthunjaya. The Stewart Platform Manipulator: A Review, *Elsevier Mechanism and Machine Theory*, 2000, pp. 15–40.
- [7] Z. Wang, J. He, H. Shang, H. Gu, Forward kinematics analysis of a six-DOF Stewart platform using PCA and NM algorithm, *Emerald Ind. Robot An Int. J.* (no. 36/5) (2009) 448–460.
- [8] X. Huang, Q. Liao, S. Wei, X. Qiang, S. Huang, X. Huang, Q. Liao, S. Wei, X. Qiang, S. Huang, Forward kinematics of the 6-6 Stewart platform with planar base and platform using algebraic elimination, in: *Proceedings of the IEEE International Conference on Automation and Logistics*, 2007, pp. 2655–2659.
- [9] K. Harib, K. Srinivasan, *Kinematic and Dynamic Analysis of Stewart Platform-based Machine tool Structures*, 21, Cambridge University Press - Robotica, 2003, pp. 541–554.
- [10] G.A. Leonov, P.E. Tovstik, T.M. Tovstik, Workspaces of the Stewart platform in the 6D space of generalized coordinates, *Vestnik St. Petersburg. Univ. Math.* (50) (2017) 180–187.
- [11] S.H. Lee, J.B. Song, W.C. Choi, D. Hong, Position control of a Stewart platform using inverse dynamics control with approximate dynamics, *Pergamon Mechatron.* (13) (2003) 605–619.
- [12] The Modelica Association, *Modelica 3.2.2 Language Specification*, The Modelica Association, Munich, Germany, 2014.
- [13] "Modelica Standard Library, v3.2.2" The Modelica Association, 03/04/2016 [Online]. Available: modelica.org/libraries. [accessed 10/02/19].
- [14] DYMOLA, "Version 2020", Dassault Systèmes, 01/01/2020, [Online]. Available: 3ds.com/products-services/catia/products/dymola/ [accessed 25/03/2020].
- [15] M. Tiller, P. Bowles, M. Dempsey, Development of a vehicle model architecture in Modelica, in: *Proceedings of the 3rd International Modelica Conference*, 2003, pp. 75–86.
- [16] G. Bardaro, L. Bascetta, F. Casella, M. Matteucci, Using Modelica for advanced multi-body modelling, in: *Proceedings of the 12th International Modelica Conference*, 2017, pp. 887–894.
- [17] S. Trabucchi, F. Casella, T. Maioli, C. Elsidio, D. Franzini, M. Ramond, Preliminary analysis of the PreFlexMS molten salt once-through steam generator, *AIP Conf. Proc.* (1850) (2017).
- [18] D. Qin, J. Li, T. Wang, Modeling and simulating a battery for an electric vehicle based on Modelica, *Automot. Innov.* 2 (2019) 169–177.
- [19] R. Ponciroli, A. Bigoni, A. Cammi, S. Lorenzi, L. Luzzi, Object-oriented modelling and simulation for the ALFRED dynamics, *Prog. Nucl. Energy* 71 (2014) 15–29.
- [20] C. Tripodo, A.D. Ronco, S. Lorenzi, A. Cammi, Development of a control-oriented power plant simulator for the molten salt fast reactor, *EPJ Nucl. Sci. Technol.* 5 (2019).
- [21] R. Ponciroli, A. Cammi, S. Lorenzi, L. Luzzi, A preliminary approach to the ALFRED reactor control strategy, *Prog. Nucl. Energy* 71 (2014) 15–29.
- [22] C. Tripodo, S. Lorenzi, A. Cammi, Definition of model-based control strategies for the molten salt fast reactor, *Elsevier Nucl. Eng. Des.* (373) (2021).
- [23] "OpenModelica," OpenModelica, 01/01/2020 [Online]. Available: openmodelica.org/ [Accessed 25/03/2021].
- [24] G. Micciché and, et al., The Remote Handling System of IFMIF-DONES, *Fusion Eng. Des.* 146 (2019) 2786–2790.
- [25] "International Fusion Material Irradiation Facility - DEMO Oriented Neutron Source," IFMIF-DONES, 01/10/2014 [Online]. Available: ifmifdones.org/ [Accessed 15 08 2021].
- [26] "LinearSystems2," The Modelica Association, 28/10/2021 [Online]. Available: ithub.com/modelica/Modelica_LinearSystems2 [Accessed 05/11/2021].
- [27] D. Özdemir, T. Motschke, W. Herfs, C. Brecher, Modelica library for feed drive systems, in: *Proceedings of the 11th International Modelica Conference*, Versailles, France, 2015.
- [28] P. Krause, O. Wasynczuk, S.D. Sudhoff, S. Pekarek, *Analysis of Electric Machinery and Drive Systems*, Wiley-IEEE Press, Piscataway, NJ, 2013.
- [29] B. Siciliano, O. Khatib, *Handbook of Robotics*, 2nd ed., Springer, 2016.
- [30] B. Siciliano, L. Sciacivico, L. Villani, G. Oriolo, *Robotics: Modelling, Planning and Control*, Springer, 2009.
- [31] F. Percacci, M. Tanaskovic, W. Kong, C. Zhao, P. Gnos, Dual loop position control for mechanical systems with backlash and elasticity, *IKMT 2019 - Innovative Small Drives Micro-Motor Syst.* (12) (2019) 1–6.
- [32] "MATLAB R2020a," The MathWorks, Inc., 01/01/2020 [Online]. Available: mathworks.com/products/matlab.html [Accessed 25 03 2020].

Further reading

- [1] C. Tripodo, Finalization/Improvement of Local Control System (LCS) design for the Parallel Kinematics Manipulator (PKM), *EUROfusion IDM*, 30/11/2020. [Online]. Available: idm.euro-fusion.org/default.aspx?uid=2PH8NE.